nature microbiology

Resource

https://doi.org/10.1038/s41564-023-01581-x

High-throughput transcriptomics of 409 bacteria–drug pairs reveals drivers of gut microbiota perturbation

Received: 6 March 2023

Accepted: 8 December 2023

Published online: 17 January 2024

Check for updates

Deirdre Ricaurte[1,2,4], Yiming Huang[1,2,4], Ravi U. Sheth[1,2], Diego Rivera Gelsinger[1], Andrew Kaufman[1] & Harris H. Wang[1,3]

Many drugs can perturb the gut microbiome, potentially leading to negative health consequences. However, mechanisms of most microorganism–drug responses have not been elucidated at the genetic level. Using high-throughput bacterial transcriptomics, we systematically characterized the gene expression profiles of prevalent human gut bacteria exposed to the most frequently prescribed orally administered pharmaceuticals. Across >400 drug–microorganism pairs, significant and reproducible transcriptional responses were observed, including pathways involved in multidrug resistance, metabolite transport, tartrate metabolism and riboflavin biosynthesis. Importantly, we discovered that statin-mediated upregulation of the AcrAB-TolC efflux pump in Bacteroidales species enhances microbial sensitivity to vitamin A and secondary bile acids. Moreover, gut bacteria carrying *acrAB-tolC* genes are depleted in patients taking simvastatin, suggesting that drug–efflux interactions generate collateral toxicity that depletes pump-containing microorganisms from patient microbiomes. This study provides a resource to further understand the drivers of drug-mediated microbiota shifts for better informed clinical interventions.

Today, half of all Americans take at least one prescription drug, with national spending predicted to reach US$400 billion by 2025[1,2]. The prevalent use of pharmaceuticals is a major contributor to the alarming shifts in the gut microbiome, especially in industrialized countries[3,4]. A recent screen of >1,000 orally administered drugs revealed a high frequency of antibacterial activity among human-targeted medications (24%), especially antipsychotics[5]. Clinically, proton pump inhibitors and atypical antipsychotics often trigger microbiota changes, with side effects resembling those of antibiotic use (for example, diarrhoea, fungal infection)[5,6]. Even though the top three prescribed drug classes (that is, antihyperlipidaemic agents, antidepressants and analgesics[7]) are all linked to gut microbiota disturbances, the mechanisms driving these shifts are poorly understood[5]. Physiologically, altered microbiome composition can negatively impact epithelial integrity[8], gut motility[9], nutrient availability[10], immune homeostasis[11,12] and even treatment response. For instance, depletions in gut bacterial diversity have been linked to worse outcomes in immunotherapy drug trials[13] and higher susceptibility to infection by pathogens such as *Clostridioides difficile*[14].

Gut microorganisms interact with pharmaceutical compounds in a variety of ways. Bacteria can biotransform drugs to impact efficacy[15,16], bioavailability[17] and toxicity[18]. For example, commensal *Eggerthella lenta* inactivates digoxin, an orally delivered cardiac glycoside, by expressing the cardiac glycoside reductase (*cgr*) operon[15]. Gut bacteria can also deplete xenobiotics from their local environment via

[1]Department of Systems Biology, Columbia University, New York, NY, USA. [2]Integrated Program in Cellular, Molecular, and Biomedical Studies, Columbia University, New York, NY, USA. [3]Department of Pathology and Cell Biology, Columbia University, New York, NY, USA. [4]These authors contributed equally: Deirdre Ricaurte, Yiming Huang. e-mail: harris.wang@columbia.edu

bioaccumulation[19] and mitigate the effects of toxic medications by using conserved antibiotic resistance mechanisms[5]. Within minutes of xenobiotic exposure, microorganisms often exhibit highly specific transcriptional responses[20,21]. Therefore, transcriptomic measurements can help quickly dissect specific drug–microorganism responses (for example, digoxin[15], 5-fluorouracil[22] and levodopa[23]). However, the current cost and scale of bacterial transcriptomics has precluded high-throughput studies from using this approach[24].

Here we describe the systematic transcriptomic analysis of 409 drug–microorganism pairs to dissect gene-level gut bacterial responses to top pharmaceuticals. We developed a high-throughput transcriptomics pipeline for optimization in non-model gut microorganisms that was then applied to generate a total of 978 individual drug–microorganism samples (including replicates). By analysing the transcriptomes of prevalent human gut bacteria exposed to top-prescribed orally administered drugs, we observed shared and strain-specific responses, including in pathways for drug degradation, vitamin biosynthesis and multidrug efflux. Further analysis of a human microbiome cohort dataset confirmed the clinical significance of our findings. This study highlights the utility of large-scale transcriptomics for functional discovery of gut microbiota–xenobiotic interactions.

Results

Transcriptomic map of microbial responses to top medicines

Of the top 200 drugs prescribed today, 83% are orally delivered and expected to interact directly with the gut microbiome[5,25,26]. We therefore sought to measure the transcriptomic responses of prevalent gut bacteria exposed to top-prescribed oral pharmaceuticals. We implemented and optimized a multiplexed RNA sequencing (RNA-seq) technique[27] for high-throughput transcriptomics of non-model gut bacteria and incorporated cost-efficient ribosomal RNA (rRNA) depletion for diverse non-model gut bacteria that we previously developed[24] (Fig. 1a). This modified pipeline can generate high-quality transcriptomes for diverse gut bacterial phyla at a cost of <US$16 for ~1 million reads per sample (Supplementary Table 1).

We assembled a panel of 14 representative and highly prevalent[28–30] human gut isolates spanning the Bacteroidetes, Firmicutes, Actinobacteria and Proteobacteria phyla (Supplementary Fig. 1 and Supplementary Tables 2 and 3) and 19 oral drugs from the top-prescribed drugs in 2017 according to the Agency for Healthcare Research and Quality (Supplementary Table 4 and Methods)[31]. Our drug list included the top eight most prescribed drugs as well as ten additional neurotransmitter modulators, which were included owing to established associations between the psychotherapeutic drug class and microbiota compositional changes[5]. Lenalidomide, a chemotherapeutic with the largest market cap in the small-molecule drug class[31], was also added.

We first assessed the antimicrobial activity of the chosen drugs against our bacterial panel (Fig. 1b, Supplementary Fig. 2 and Methods). Drug concentrations were chosen to span median drug concentrations within the small intestine and large intestine, which have been estimated to approach 20 and 100 μM, respectively[5]. We did not observe growth inhibition for most strains at 2 or 20 μM concentration (Supplementary Fig. 2). At 100 μM, growth inhibition was observed for at least one drug in 18 of 19 strains within 24 h (Fig. 1b). Notably, *Bifidobacterium longum* did not exhibit growth defects in any drug condition. Broad-spectrum antimicrobial activity was seen for simvastatin, amlodipine and a subset of psychotherapeutics (that is, sertraline, paroxetine, duloxetine and fluoxetine), in agreement with previous reports[5]. Interestingly, we observed the greatest magnitudes of drug-induced growth defects within Bacteroidetes strains, suggesting that these species are more susceptible to drug toxicities (Fig. 1b and Supplementary Fig. 2). We further validated that the observed toxicity profiles extended to complex bacterial communities by exposing the drug panel to a fresh faecal sample from a healthy volunteer. We observed similar growth inhibition profiles of 13 panel strains grown in the faecal community (Supplementary Fig. 3), supporting the relevance of our individual strain-level growth measurements in the context of a complex consortium.

As substantial growth inhibition can confound transcriptional measurements, we performed all subsequent transcriptomic assays at 20 μM, which reasonably approximated intestinal drug concentrations for detecting drug responses while minimizing drug toxicities[5,32]. To further avoid the impact of antimicrobial toxicity, cells were collected at 1.5 h post-exposure, which is shorter than the doubling time of several gut bacteria[33]. The transcriptomic pipeline was first validated using *Eggerthella lenta* exposed to our drug panel, as well as digoxin as a positive control (Supplementary Figs. 4 and 5 and Supplementary Table 5). Differential *Eggerthella lenta* gene expression was observed in 17 of 20 drug conditions, including the expected upregulation of the *cgr* operon by digoxin[15] (Supplementary Fig. 5). The transcriptomic pipeline was thus applied to all drug–microorganism pairs in biological duplicates (Supplementary Fig. 4b and Supplementary Tables 6–8).

Overall, substantial and consistent transcriptional responses were observed across drug classes and bacterial phyla (Supplementary Table 6). We used the magnitude of global transcriptional response as a common proxy[34] by calculating the ratio of differentially expressed genes (DEGs) to the total gene count per genome, which we refer to as the DEG ratio or DEGR (Fig. 1c). All drugs produced differential expression in at least one strain. The largest aggregate DEGR was produced by simvastatin (0.014), followed by sertraline (0.010), levothyroxine (0.006) and paroxetine (0.004) (Fig. 1c, top bars). Notably, in many cases, drugs eliciting large global transcriptional changes also exhibited broad-spectrum toxicity in the growth screen (Fig. 1b,c and Supplementary Fig. 6).

Large transcriptional changes are often associated with expression changes of global regulators and transcription factors (TFs)[35]. Indeed, the drug–microorganism pairings associated with the highest DEGRs (simvastatin–*Bacteroides stercoris*, sertraline–*Fusicatenibacter saccharivorans*, simvastatin–*Alistipes shahii*) also induced the highest numbers of TFs (14, 13 and 12, respectively) (Supplementary Fig. 7). However, in several cases, bacterial–drug exposures generated differential expression without TF modulation, such as *Dorea longicatena* exposed to metoprolol tartrate and *Phocaeicola dorei* exposed to various selective serotonin reuptake inhibitors (SSRIs) (Supplementary Fig. 7). In these cases, differential expression was not consistently correlated with antimicrobial activity (Fig. 1b,c). These results indicate that drug–microorganism exposures producing large and broad gene expression changes often correlate with drug toxicity, while those eliciting specific transcriptional responses may not.

To understand the functional impact of different exposures on the gut microbiota, we performed pathway enrichment analysis using the Kyoto Encyclopedia of Genes and Genomes (KEGG) database to classify DEGs across the drug panel, agnostic of strain identity (Fig. 2). Most differentially regulated modules (adjusted *P* value (P_{adj}) < 0.01, fold change (FC) > 4) were associated with mechanisms of antibiotic resistance (Fig. 2a). Specifically, pathways related to multidrug resistance, transport and two-component systems were enriched. Simvastatin, sertraline and amlodipine—the drugs exhibiting the broadest toxicity in growth screens—strongly upregulated multidrug resistance pathways associated with efflux transporters. Furthermore, trazodone and levothyroxine, which triggered differential expression in Bacteroidetes, Firmicutes and Actinobacteria without impacting growth (Fig. 1b,c), showed similarly enriched pathways to more toxic screened compounds (Fig. 2a). While growth deficits were not detected in trazodone- and levothyroxine-treated cultures at the maximum concentrations, this result suggests that these compounds could exhibit toxicity in vivo at concentrations exceeding 100 μM. Notably, post-treatment microbiota changes have been detected in hypothyroid patients taking levothyroxine[36] and psychiatric patients taking trazodone[37].

https://doi.org/10.1038/s41564-023-01581-x

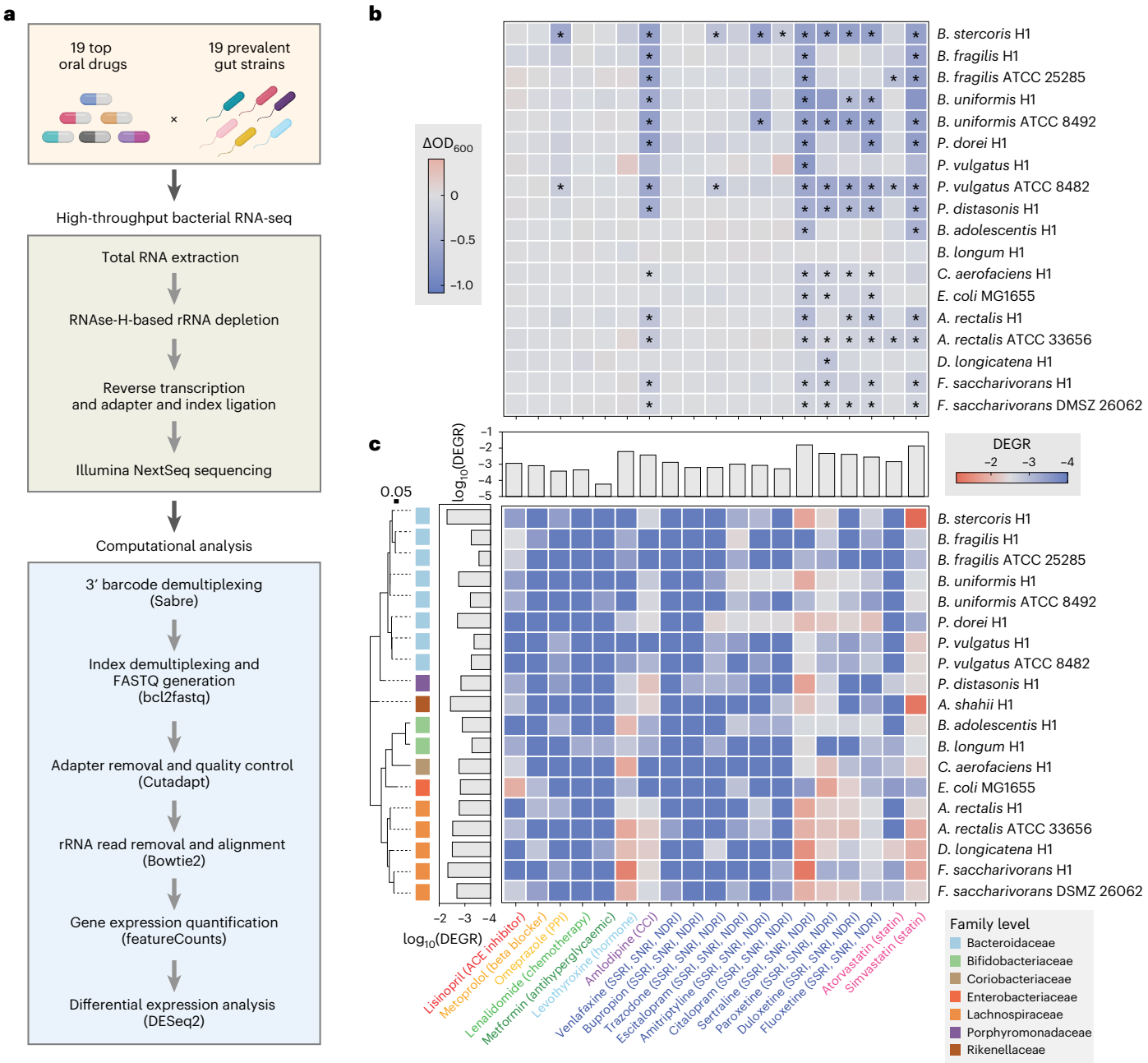

Fig. 1 | Top-prescribed drugs elicit rich transcriptomic responses from prevalent gut bacterial species. a, Schematic of our high-throughput transcriptomic pipeline for non-model gut microorganisms. **b**, The heat map colour indicates the delta in average OD at 48 h of bacterial strain growth in mGAM supplemented with different pharmaceuticals at 100 μM as compared to a same-volume solvent control ($n = 3$ per condition). Drug condition is indicated on the *x*-axis, and strain identity is indicated on the *y*-axis. Asterisks indicate >0.3 average absolute change in growth with $P_{adj} < 0.05$, calculated using two-sided independent *t*-test with Benjamini–Hochberg correction. **c**, Bacterial strains were exposed to drugs ($n = 2$ per condition) or vehicle controls ($n = 4$ per condition), and differentially expressed genes ($P_{adj} < 0.05$, calculated as above) were identified. The heat map colour represents the $\log_{10}$ value of the DEGR, defined as the number of differentially expressed genes in a drug condition divided by the total number of genes within a strain genome, with the drug indicated on the *x*-axis (classes grouped by colour) and strain identity indicated on the *y*-axis. The bar plot inserts show $\log_{10}$ values of average DEGRs across strains (top bar plot insert) or drugs (left bar plot insert). A maximum likelihood phylogenetic tree is shown on the left with bacterial family identity indicated by colour in the figure legend. PPI, proton pump inhibitor; CCI, calcium channel inhibitor; SSRI, selective serotonin reuptake inhibitor; SNRI, serotonin norepinephrine reuptake inhibitor; NDRI, norepinephrine-dopamine reuptake inhibitor.

We next examined functional orthologues within pathways that exhibited the greatest magnitudes of differential regulation across drug conditions (Fig. 2b). Among the top seven most upregulated orthologues, six corresponded to conserved multidrug efflux pumps (Fig. 2b). Among these orthologues, the top four (HAE1, AcrA, mexK and oprM) belonged to the Resistance–Nodulation–Division permease superfamily, a drug and heavy metal efflux system whose upregulation is associated with gram-negative bacterial antibiotic resistance[38,39]. The fifth and sixth orthologues (bcrB and ABCB-BAC) belonged to the ATP-binding cassette (ABC) superfamily, which was also highly represented among the top downregulated orthologues across drug conditions (Fig. 2b). Interestingly, the ABC superfamily is not considered to

https://doi.org/10.1038/s41564-023-01581-x

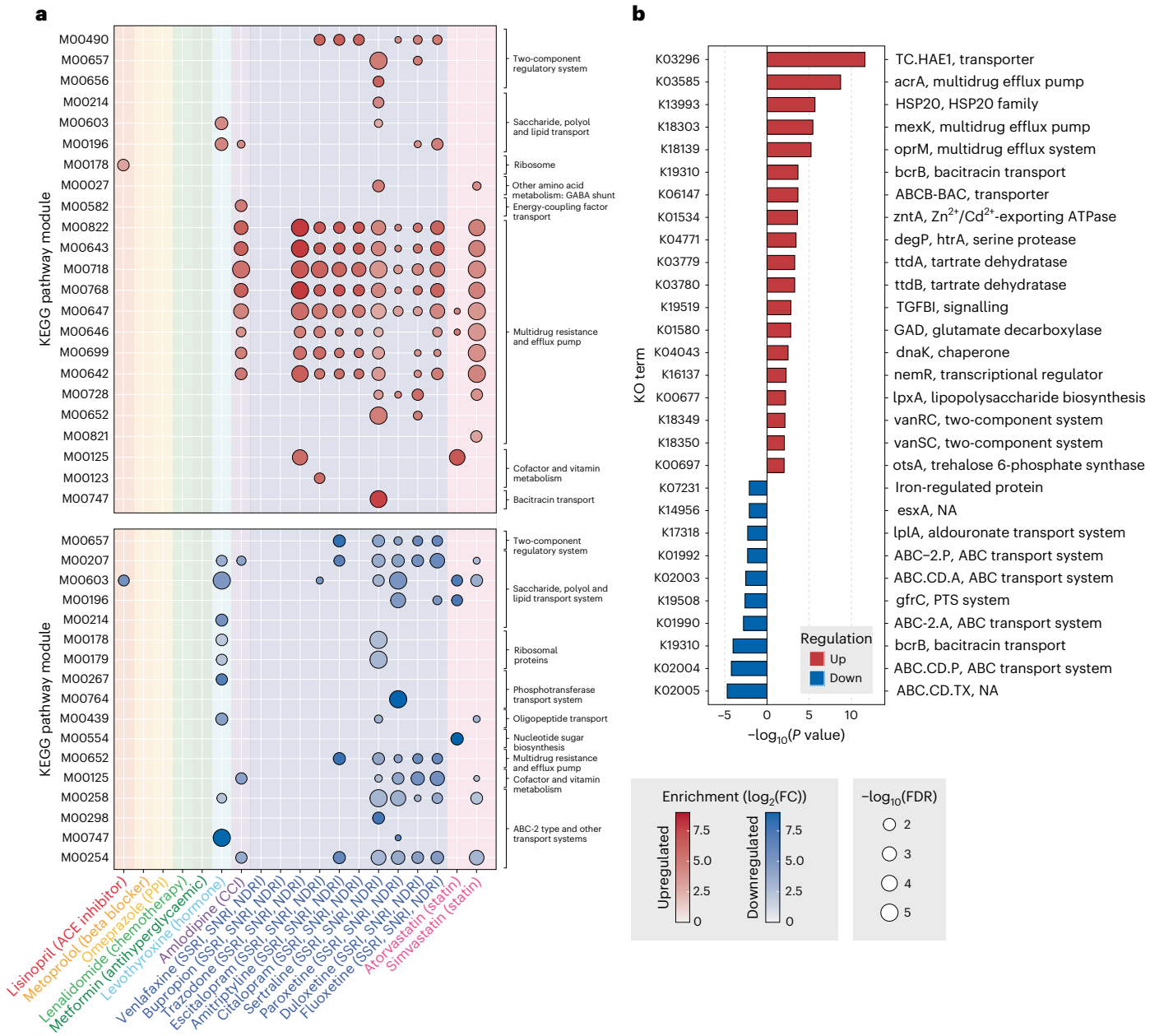

Fig. 2 | Pathway enrichment analysis reveals modulation of conserved efflux pathways by top pharmaceutical compounds. a, KEGG modules with significant enrichment ($P_{adj} < 0.05$ by two-sided independent *t*-test with Benjamini–Hochberg correction, *e* value < 10^{-5}) based on pathway analysis of DEG datasets are shown. The drug condition is shown on the *x*-axis, with the colour of each drug condition corresponding to the background colour of the bubble plot. Identifiers (IDs) of KEGG modules with significant enrichment are shown on the left *y*-axis, and KEGG pathway groups are shown on the right *y*-axis. The bubble colour indicates the direction of regulation (red, upregulation; blue, downregulation), the bubble intensity indicates $\log_2$(FC) enrichment and the bubble size indicates the level of significance ($-\log_{10}(P_{adj})$). **b**, Top 19 upregulated and top 10 downregulated functional orthologues within the DEG dataset across drugs, as annotated within the KEGG Orthology (KO) database. The bar colour indicates the direction of transcriptional regulation as in **a**. $-\log_{10}(P_{adj})$, calculated as in **a**, is shown on the *x*-axis. The K number assigned by the KO database is shown on the left *y*-axis, and the putative orthologue function is shown on the right *y*-axis.

contribute substantially to bacterial multidrug resistance; however, these pumps are highly associated with chemotherapy resistance in eukaryotic cells[40]. Together, these observations suggest that gut bacterial strains use conserved multidrug efflux pumps to ameliorate toxicities of human-targeted drug compounds[5].

Given the link between the identified Resistance–Nodulation–Division-type efflux pumps and antibiotic resistance in gram-negative species[38,39], we wondered whether gut bacteria use the same resistance pathways to ameliorate toxicities in commonly prescribed antibiotic classes. To explore this question, we generated transcriptomes for four species (*Agathobacter rectalis* H1, *D. longicatena* H1, *B. longum* H1 and *Phocaeicola vulgatus* H1) exposed to seven commonly prescribed antibiotics that target bacterial synthesis of DNA (ciprofloxacin), proteins (tetracycline, streptomycin and erythromycin) or the cell membrane (cefotaxime, ampicillin and vancomycin) (Supplementary Figs. 4 and 8 and Supplementary Table 9). Principal coordinates analysis (PCoA) revealed that transcriptomic responses to traditional antibiotics clustered by drug target across sensitive strains (*A. rectalis*,

https://doi.org/10.1038/s41564-023-01581-x

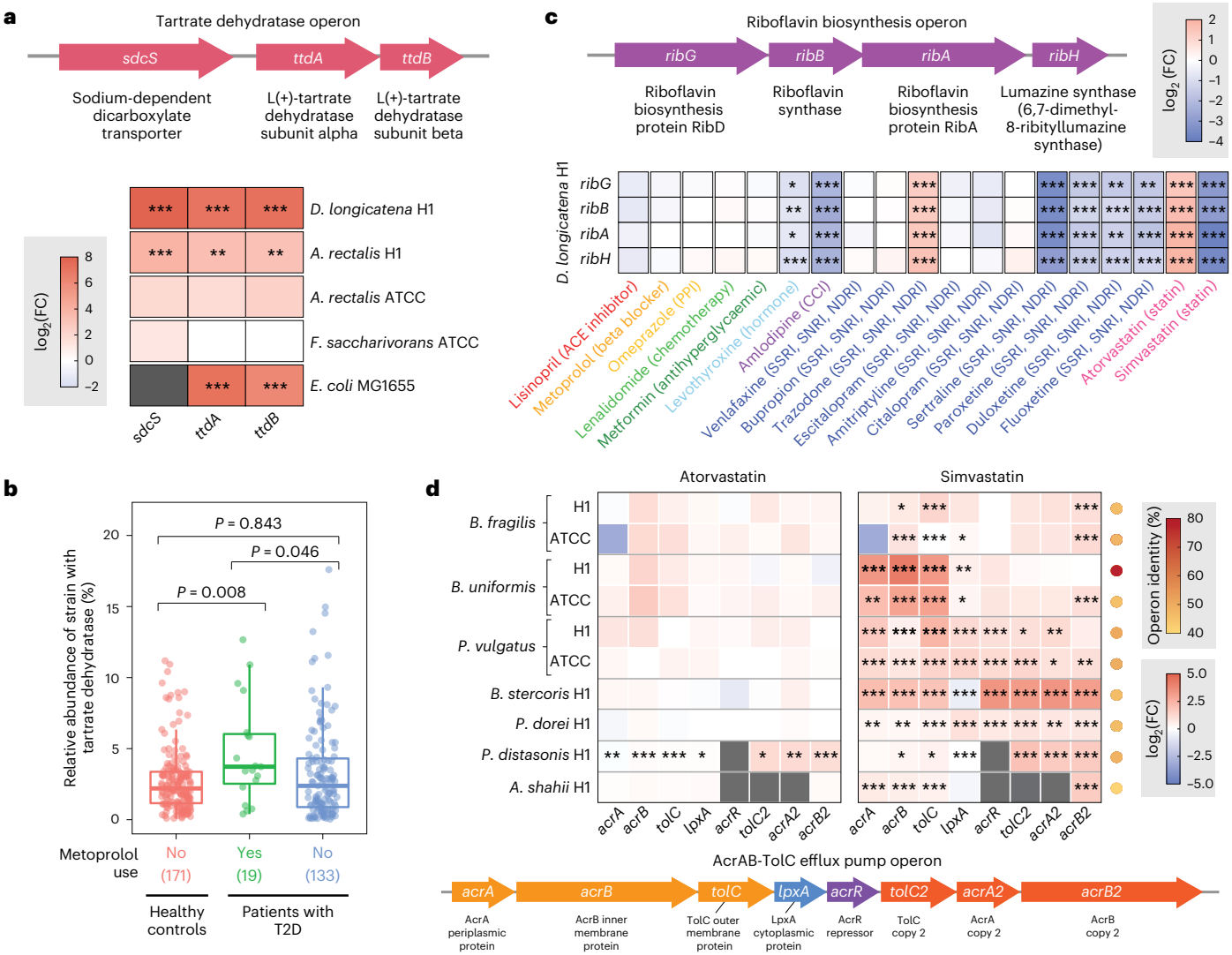

Fig. 3 | Top pharmaceutical compounds impact gut bacterial metabolism, vitamin production and mitigation of toxic metabolites. a, The top schematic shows the components of the tartrate dehydratase (*ttd*) operon in *Escherichia coli*. Genes within the operon are shown on the *x*-axis, and isolates containing *ttd* analogues are shown on the *y*-axis. The heat map colour indicates $\log_2$(FC) in TPM expression. $^*P_{adj} < 0.05$; $^{**}P_{adj} < 0.01$; $^{***}P_{adj} < 0.001$, calculated by two-sided independent *t*-test with Benjamini–Hochberg correction. Grey panels indicate the absence of a gene analogue. **b**, The relative abundance of bacterial isolates containing the *ttd* operon was calculated within a dataset of patients with T2D[48] ($n = 323$ total patients). The *x*-axis indicates patient cohorts, grouped by healthy controls not taking metoprolol (red dots), patients with T2D taking metoprolol (green dots) and patients with T2D not taking metoprolol (blue dots). The relative abundance of isolates is shown on the *y*-axis as a box and whisker plot. Box hinges correspond to the 25th and 75th percentiles, and whiskers extend to values within 1.5 of the interquartile range (outliers omitted). *P* values calculated using two-sided independent *t*-test are annotated with brackets. **c**, The top schematic shows the components of the riboflavin biosynthesis (*rib*) operon in *D. longicatena* H1. Drugs are shown on the *x*-axis (grouped and coloured by class), and gene components of the *rib* operon are shown on the *y*-axis. The heat map colours indicate $\log_2$(FC) in TPM expression. The asterisks indicate significance as calculated and annotated in **a**. **d**, Regulation of *acrAB-tolC* within Bacteroidales isolates by atorvastatin and simvastatin. The bottom schematic shows the components of the *acrAB-tolC* operon in *Escherichia coli*. Genes within *acrAB-tolC* are shown on the *x*-axes, and isolates containing AcrAB-TolC analogues are shown on the *y*-axis. Heat map colours indicate $\log_2$(FC) in TPM expression, as indicated by the bottom-right red-to-blue colour bar. Asterisks indicate significance as calculated and annotated in **a**. Dots to the right of the strain rows indicate percentage of operon identity compared with the *P. vulgatus* AcrAB-TolC reference[57], as indicated by the top right red-to-yellow colour bar.

D. longicatena, *P. vulgatus*), suggesting that bacteria use conserved pathways to mitigate toxicities of drugs with similar bacterial targets (Supplementary Fig. 8a). Notably, minimal transcriptomic responses to streptomycin exposures were observed, consistent with the inherent streptomycin resistance of anaerobically grown bacterial isolates[41]. Furthermore, *B. longum*, the only bacterial strain in our panel that did not exhibit growth sensitivity to at least one screened pharmaceutical, showed minimal transcriptional responses to antibiotic exposures compared with a vehicle control, a behaviour consistent with resistance[32]. To compare bacterial pathways induced by traditional antibiotic exposures, we next performed a KEGG pathway enrichment analysis of DEGs in the four tested bacteria exposed to orally delivered drugs or traditional antibiotics (Supplementary Fig. 8b). Membrane-directed antibiotics upregulated pathways associated with cell membrane synthesis and modification (vancomycin resistance, fatty acid synthesis pathways), while ribosomal-targeted antibiotics induced upregulation of ribosomal pathways and downregulation of ATP synthesis. Remarkably, our analysis revealed no overlap in bacterial pathways induced by non-antibiotic pharmaceuticals and traditional antibiotic compounds, suggesting that non-antibiotic orally

delivered compounds impact unique mechanisms of prokaryotic multidrug resistance.

Drugs impact gut bioavailability, biosynthesis and toxicity

To obtain a deeper functional understanding of bacterial–drug interactions at the operon level, we searched for clusters of DEGs transcribed within the same operon. Numerous differentially expressed operons were identified across strains (Supplementary Table 8). Existing mechanistic studies of gut microbiota–drug interactions have identified a range of bacterial drug responses that can cause differential treatment outcomes, including drug metabolism, toxicity mitigation and alteration of the prokaryotic metabolome[5,19,42]. To explore the diversity of physiologically relevant bacterial–xenobiotic interactions, we selected three representative operons associated with drug metabolism, vitamin biosynthesis and toxicity mitigation for further examination (Fig. 3).

First, we observed the upregulation of the tartrate dehydratase (*ttd*) operon in *Escherichia coli*, *A. rectalis* and *D. longicatena* exposed to metoprolol tartrate, a beta blocker used to treat hypertension[43] (Fig. 3a). Metoprolol is chemically formulated either as metoprolol tartrate or metoprolol succinate for immediate release or extended release, respectively. Which form of metoprolol is administered can impact bioavailability, with metoprolol tartrate producing higher peak-to-trough variation among patients[44]. For bacteria, dietary tartrate metabolism through the *ttd* operon provides another carbon source in the gastrointestinal tract[45]. Our results suggest that certain gut microorganisms can metabolize the tartrate salt of immediate-release metoprolol, which could contribute to fluctuations in drug bioavailability within patient cohorts. These findings could also have broader implications for other tartrate-conjugated drugs[46]. Furthermore, upregulation of tartrate metabolism by metoprolol could have unintended negative consequences in the context of cardiovascular disease[47]. Increases in bacterial tartrate metabolism have been linked to metabolic disorders, including atherosclerotic cardiovascular disease, type 2 diabetes (T2D) and obesity[47]. Enrichment in tartrate metabolism has also been associated with higher abundance of *Escherichia coli*, a metoprolol tartrate metabolizer identified in our screen. Using a published clinical metagenomic microbiome dataset of patients with T2D[48], we performed an additional analysis exploring the distribution of *ttd* genes among patients with T2D consuming metoprolol. We found that patients with T2D taking metoprolol had an increased abundance of the *ttd* operon in their gut metagenome compared with patients not taking metoprolol ($P = 0.046$) and healthy controls ($P = 0.008$; Fig. 3b). Therefore, our findings combined with previous studies suggest that treatment with metoprolol tartrate for hypertension, which is the strongest predictor for atherosclerotic cardiovascular disease[49], might inadvertently influence the pathophysiology of a metabolic disorder via an increase in microbiota tartrate metabolism.

Next, we identified differential regulation of the riboflavin biosynthesis (*rib*) operon in *D. longicatena* by several drugs within our panel (Fig. 3c). The gut microbiome is an important source of riboflavin (vitamin B_2) in humans[50]. Riboflavin production is an essential pathway in bacteria, as downstream metabolites flavin mononucleotide and flavin adenine dinucleotide are co-enzymes for oxidases, reductases and dehydrogenases[51]. In gram-positive bacteria, riboflavin biosynthesis is downregulated by a flavin mononucleotide-responsive riboswitch, which also responds to roseoflavin[51]. In our transcriptomics dataset, several SSRIs (sertraline, paroxetine, fluoxetine, duloxetine), a cardiovascular medication (amlodipine), simvastatin and levothyroxine all downregulate riboflavin production in *D. longicatena*. We also observed upregulation of the *rib* operon by *D. longicatena* in response to trazodone and atorvastatin exposure. Clinically, vitamin B_2 deficiency is associated with a higher risk of psychiatric disorders for which SSRIs are indicated (for example, depression), although whether these depletions are a cause or a result of disease is not understood[52,53]. Reduced riboflavin concentrations can also contribute to hyperhomocysteinaemia, a well-studied independent risk factor for atherosclerosis[54,55]. Our data suggest that the administration of certain SSRIs and cardiovascular medications could modulate vitamin B_2 levels in the setting of mood disorders or heart disease, respectively, which could have unintended detrimental consequences on the disease state.

Finally, we observed a strong statin-mediated upregulation of genes encoding the AcrAB-TolC efflux pump in all Bacteroidales strains tested (*Bacteroides fragilis*, *B. stercoris*, *Bacteroides uniformis*, *P. dorei*, *P. vulgatus*, *Parabacteroides distasonis*, *A. shahii*; Fig. 3d). The AcrAB-TolC pump has been linked to resistance against several classes of antibiotics as well as non-antibiotic orally delivered pharmaceuticals including methotrexate and tamoxifen[5,56]. The pump is also known to mediate bacterial sensitivity to retinol and secondary bile acids[57]. Given that previous studies have linked statin use with changes in gut microbiome composition[25], we thus explored the mechanism by which upregulation of AcrAB-TolC by statins could impact microbial physiology in the gut.

Statins modulate AcrAB-TolC activity in gut microorganisms

Statins have been widely studied for their potential as non-traditional antibiotics, with simvastatin garnering particular attention for its activity against multidrug-resistant pathogens such as *Staphylococcus aureus*[58]. Simvastatin alters the composition of gut microbiome in patients, but the mechanism driving this microbial shift is not understood[25]. In our transcriptomic screening, we found that simvastatin strongly upregulated *acrAB-tolC* genes across multiple Bacteroidales strains, while atorvastatin significantly upregulated *acrAB-tolC* genes only in *P. distasonis* (Fig. 3d). Interestingly, these transcriptional profiles correlated with strong and modest toxicities exhibited in our growth screens by simvastatin and atorvastatin, respectively (Fig. 1b), motivating further exploration into the role of AcrAB-TolC in the interplay between gut microorganisms and antimicrobial compounds.

In *Bacteroides* species, the AcrAB-TolC efflux pump ameliorates the toxicity of antibiotics and common dietary metabolites such as retinol (vitamin A)[57]. We thus hypothesized that drugs altering AcrAB-TolC expression in Bacteroidales species could result in targeted changes in the toxicity of other compounds. Using *P. distasonis*, we first determined the minimum inhibitory concentration (MIC) of retinol (>24 μg ml^{-1}) and several common antibiotics with different mechanisms of action whose resistance is mediated by AcrAB-TolC[56] (Supplementary Table 10). In the presence of simvastatin, the MICs of several of these compounds were significantly shifted, with retinol showing the most pronounced effect (>2-fold decrease; Supplementary Fig. 9). We then exposed four Bacteroidales strains (*P. distasonis* H1, *P. dorei* H1, *P. vulgatus* H1 and *P. vulgatus* ATCC 8482) to retinol in the presence or absence of statins and additional drugs (sertraline, trazodone, amlodipine) observed to upregulate the *acrAB-tolC* operon (Fig. 4a and Supplementary Fig. 10). As a negative control, retinol-exposed non-Bacteroidales strains (*Escherichia coli*, *A. rectalis*, *D. longicatena*) were co-incubated with simvastatin (Supplementary Fig. 11). At 20 μM, simvastatin enhanced the sensitivity to retinol in all Bacteroidales strains, with the strongest shift seen in *P. distasonis* and *P. vulgatus* (fourfold reduction in MIC; Fig. 4a). In non-Bacteroidales strains (*Escherichia coli*, *D. longicatena*, *A. rectalis*), retinol MICs were not significantly altered by simvastatin co-incubation (Supplementary Fig. 11). Notably, we observed a modest shift approaching significance in simvastatin-treated *A. rectalis*, which we attribute to combined global toxicity burdens of simvastatin and retinol, unrelated to the AcrAB-TolC pump. Sertraline modestly increased retinol sensitivity in all Bacteroidales strains, amlodipine showed similar effects in two of four strains (*P. vulgatus* H1 and *P. dorei* H1), atorvastatin modestly decreased the MIC of retinol in *P. distasonis* only and trazodone did not significantly influence the MIC of retinol in any strains (Fig. 4a and Supplementary Fig. 10).

Deoxycholic acid (DCA) is a secondary bile acid whose toxicity is also modulated by AcrAB-TolC[57]. We thus tested whether simvastatin

https://doi.org/10.1038/s41564-023-01581-x

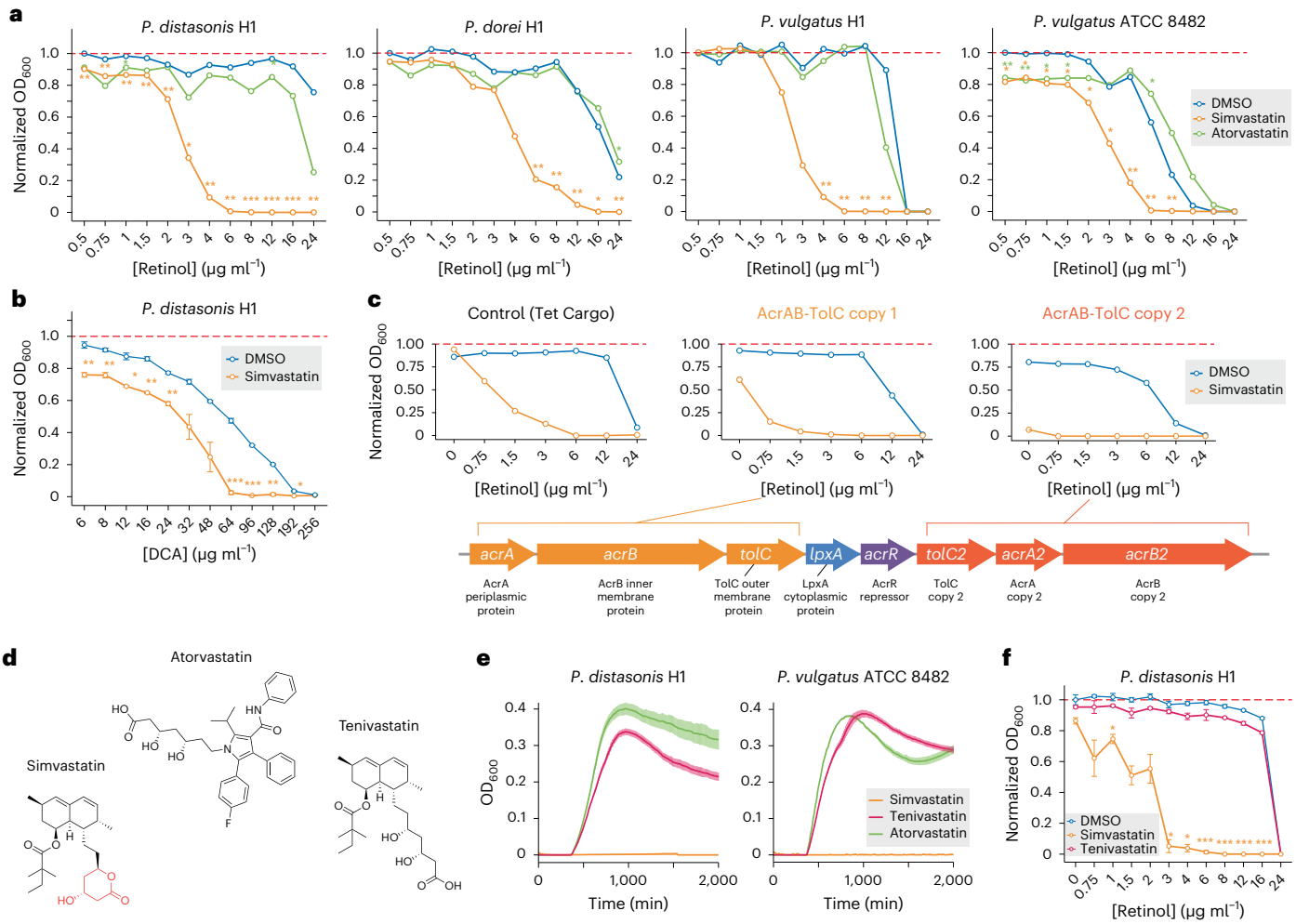

Fig. 4 | Statin exposure alters *Bacteroides* sensitivity to common dietary metabolites via the AcrAB-TolC efflux pump. a, Bacteroidales isolates exposed to retinol at various concentrations in the presence of 20 μM simvastatin (orange lines), atorvastatin (green lines) or vehicle control (blue lines). Graph titles indicate strain identity, with retinol concentration shown on the *x*-axis and growth (OD_{600}) relative to a vehicle control shown on the *y*-axis. **b**, *P. distasonis* H1 exposed to various DCA concentrations in the presence of 20 μm simvastatin (orange lines) or vehicle control (blue lines). Bile acid concentration is shown on the *x*-axis, and growth relative to a vehicle control is shown on the *y*-axis. Standard deviation bars ($n = 3$ biologically independent culture replicates per condition) are shown; $^{*}P_{adj} < 0.05$; $^{**}P_{adj} < 0.01$; $^{***}P_{adj} < 0.001$, calculated using two-sided independent *t*-test with Benjamini–Hochberg correction. **c**, *P. vulgatus* H1 overexpressing different copies of AcrAB-TolC (see schematic) or a plasmid control exposed to different concentrations of retinol in the presence of 20 μm simvastatin ($n = 3$ biologically independent culture replicates, orange lines) or vehicle control ($n = 3$ biologically independent culture replicates, blue lines). Retinol concentration is shown on the *x*-axis, and average OD_{600} growth across replicates relative to the average growth of vehicle controls is shown on the *y*-axis. **d**, Structures of atorvastatin, simvastatin and tenivastatin (simvastatin-hydroxy acid). The lactone ring in simvastatin is shown in red. **e**, *P. distasonis* H1 and *P. vulgatus* ATCC8482 grown in liquid mGAM supplemented with simvastatin (orange line), tenivastatin (raspberry line) or atorvastatin (green line) at 100 μM concentrations. Standard error bars ($n = 4$ biologically independent culture replicates per condition) for average OD_{600} growth across replicates are shown. **f**, *P. distasonis* H1 retinol MIC curves in the presence of 20 μM simvastatin ($n = 2$, orange line), tenivastatin ($n = 3$ biologically independent culture replicates, raspberry line) or vehicle control ($n = 3$ biologically independent culture replicates, blue line). P_{adj} values and standard deviations of average OD_{600} growth at each concentration are annotated as in **b**.

enhanced DCA toxicity in *P. distasonis*. Simvastatin at 20 μM significantly limited *P. distasonis* growth when co-incubated with DCA (MIC = 64 μg ml^{-1}, 66% reduction; Fig. 4b). Simvastatin did not lower the MIC of other secondary bile acids (that is, hydroxydeoxycholic acid and ursodeoxycholic acid) whose toxicity is not mediated by AcrAB-TolC[57] (Supplementary Fig. 12). Importantly, the simvastatin-altered MICs of retinol and DCA each fall within estimated colon concentration ranges of these metabolites in the human gut[57,59].

Having established that simvastatin significantly upregulates AcrAB-TolC in Bacteroidales species and that this exposure increases Bacteroidales sensitivity to retinol and DCA, we next sought to confirm that AcrAB-TolC upregulation directly increases sensitivity to dietary metabolites. To establish causality of AcrAB-TolC upregulation in increasing collateral sensitivity of Bacteroidales species to retinol, we engineered a *P. vulgatus* H1 isolate to overexpress different copies of AcrAB-TolC or a control cargo, and measured retinol MIC for engineered isolates exposed to simvastatin or DMSO (Fig. 4c and Methods). Compared with plasmid overexpression of a cargo control, overexpression of either copy of AcrAB-TolC increased collateral sensitivity to retinol, establishing that efflux pump overexpression directly increases collateral sensitivity to vitamin A. Notably, while minimal toxicity was associated with plasmid overexpression in the control *P. vulgatus* strain, *acrAB-tolC* expression also increased the toxicity of simvastatin at 20 μM concentrations, as exhibited by *P. vulgatus* growth at retinol concentrations of zero. Furthermore, overexpression of *acrAB-tolC* copy 2 caused greater enhancement of retinol and

https://doi.org/10.1038/s41564-023-01581-x

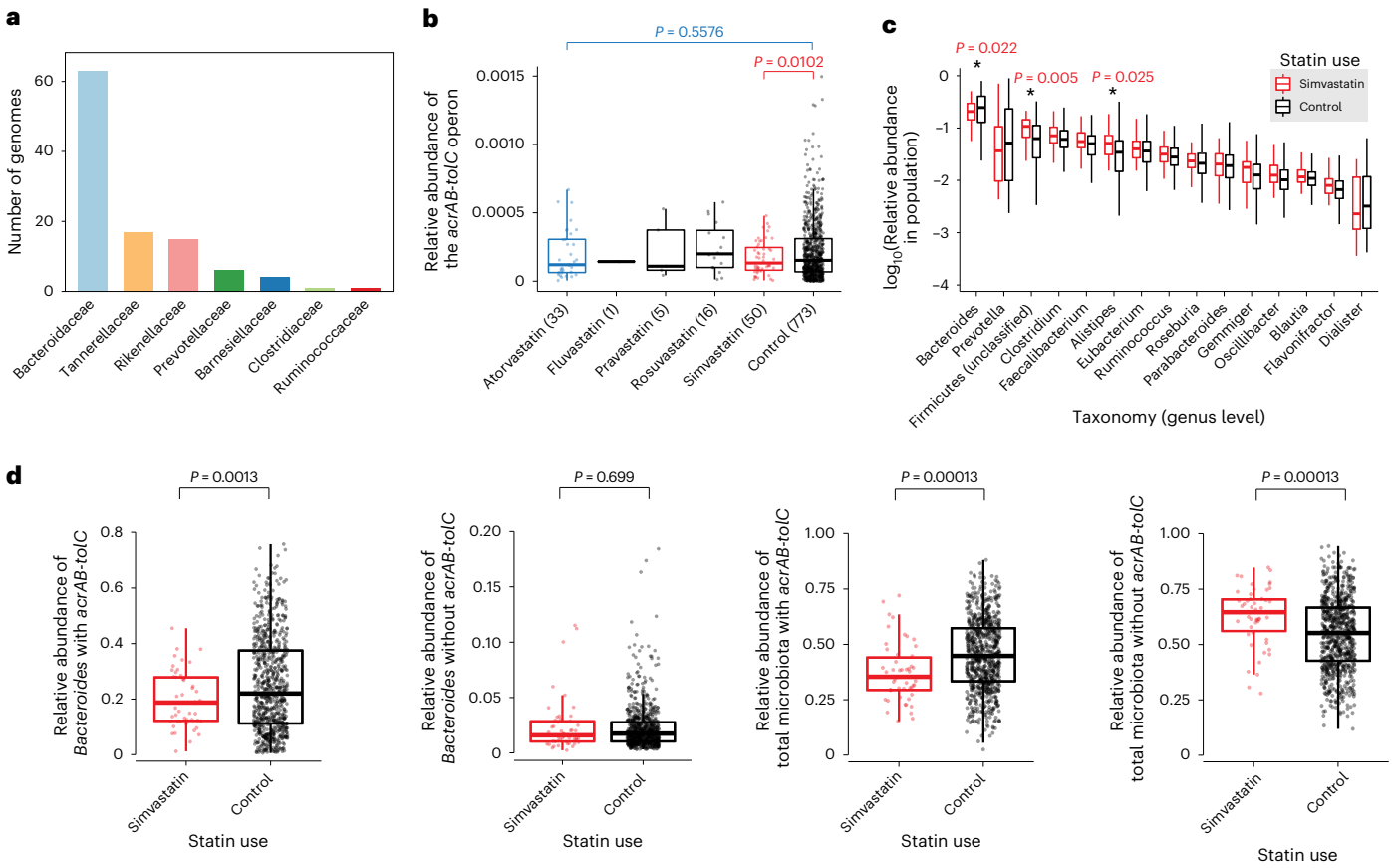

Fig. 5 | AcrAB-TolC is linked to gut microbiota shifts in statin-treated patient populations. a, The number of genomes containing *acrAB-tolC* analogues based on ref. 63. The bacterial families are indicated on the *x*-axis and by bar colour. The number of *acrAB-tolC*-containing genomes within each family is indicated on the *y*-axis. **b**, The relative abundance of *acrAB-tolC* within treatment groups of the BMIS cohort is shown as a box and whisker plot. Box hinges correspond to the 25th and 75th percentiles, and whiskers extend to values within 1.5 of the interquartile range (outliers omitted). Statin or control cohorts are indicated on the *x*-axis. Simvastatin (red) and atorvastatin (blue) cohorts are highlighted, and corresponding *P* values (calculated using two-sided independent *t*-test) are annotated with coloured brackets. Each dot represents a different patient metagenome. **c**, Relative abundance of bacterial species within the BMIS dataset, annotated using ref. 63. For each genus, the $\log_{10}$ relative abundance within simvastatin-treated (red) and non-treated (black) individuals is shown as a box and whisker plot. Box hinges correspond to the 25th and 75th percentiles, and whiskers extend to values within 1.5 of the interquartile range (outliers omitted). $^*P < 0.05$ as calculated using two-sided independent *t*-test. **d**, Relative abundance of *Bacteroides* species (left two panels) or all gut bacteria (right two panels) in simvastatin-treated and untreated individuals within the BMIS cohort. Within each panel, the *x*-axis indicates the simvastatin and the control treatment cohorts, and relative abundances of species with or without the *acrAB-tolC* operon are indicated on the *y*-axis. *P* values are annotated as in **b**.

simvastatin toxicity in *P. vulgatus* as compared with copy 1, suggesting distinct efficacy levels of these genomic efflux pump copies. Taken together, our transcriptomic dataset revealed a statin-mediated interaction with the AcrAB-TolC efflux pump that could enhance the antimicrobial effects of common dietary and host metabolites in vivo, potentially accounting for the gut microbiota alterations seen in statin-treated patient populations[25].

Simvastatin is generally administered as a lactone prodrug, while atorvastatin is administered in the active compound form[58] (Fig. 4d). Given the role of lactone moieties in many antibiotics[60], we wondered whether the transcriptional regulation of the AcrAB-TolC efflux pump by simvastatin might be linked to the toxicity of its lactone moiety. To test whether the lactone ring in simvastatin induces toxicity, we incubated simvastatin-sensitive *P. distasonis* and *P. vulgatus* strains with the lactone prodrug (simvastatin), the non-lactone activated compound (tenivastatin) and atorvastatin (Fig. 4e). Interestingly, tenivastatin, which does not contain a lactone ring, did not exhibit toxicity against either tested strain. Notably, AcrAB-TolC preferentially binds to hydrophobic substrates (for example, lipophilic lactone side chains)[61,62]. To determine whether AcrAB-TolC modulation of bacterial inhibition by dietary metabolites depends on the presence of the toxic simvastatin lactone moiety, we exposed a *P. distasonis* strain to various concentrations of retinol in the presence or absence of 20 μM simvastatin or tenivastatin (Fig. 4f). Tenivastatin did not lower the MIC of retinol, suggesting that the intact lactone ring of the unmetabolized prodrug simvastatin is necessary to enhance bacterial retinol sensitivity.

Next, to better understand the prevalence of AcrAB-TolC in the human gut microbiome, we assessed its frequency in 4,930 representative metagenome-assembled genomes (MAGs) sourced from healthy human microbiomes (Fig. 5a and Methods)[63]. A total of 106 MAGs contained a complete AcrAB-TolC homologue ($e < 10^{-5}$, coverage > 90%, identity > 40%), of which 59.4% were linked to the Bacteroidaceae family. The high prevalence of *acrAB-tolC* in Bacteroidaceae suggests that Bacteroidaceae-dominated individuals may be particularly susceptible to simvastatin-mediated microbiota changes.

To explore the clinical relevance of simvastatin-induced upregulation of the *acrAB-tolC* operon, we next quantified the metagenomic abundance of this operon's homologues in stool samples from the body mass index spectrum (BMIS) cohort[25] (Fig. 5b–d). Notably, the AcrAB-TolC pump was highly prevalent in faecal metagenomes of the BMIS cohort, with 91.6% of study participants showing >20% median relative abundance of AcrAB-TolC across treatment groups

https://doi.org/10.1038/s41564-023-01581-x

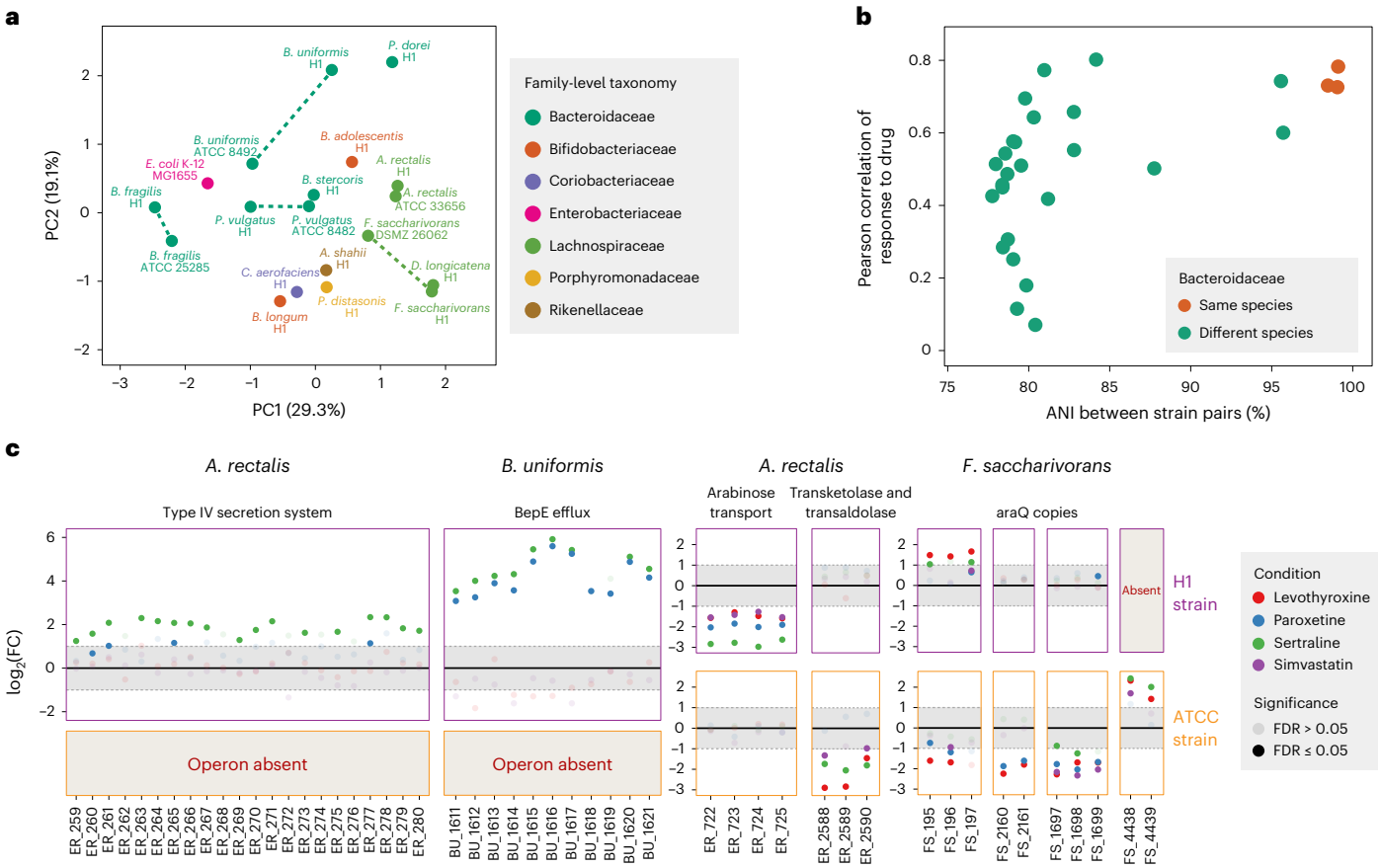

Fig. 6 | Diverse patterns of transcriptional response among conspecific bacterial isolates. a, Plot of PCoA results comparing the transcriptomic responses of tested gut bacterial isolates to top pharmaceutical compounds, using DEGRs within each drug condition as features. The variance contribution of the first and second principal coordinates is shown on the *x*- and *y*-axes, respectively. The bacterial family of each isolate is indicated by colour. Conspecific strains are connected by dotted lines. **b**, For each possible pair of Bacteroidaceae strains, a comparison of ANIs (shown on the *x*-axis) and Spearman correlation of DEGRs across all drug conditions (shown on the *y*-axis) is shown. Each dot indicates a pairwise comparison, with colour indicating whether the comparison was performed on conspecific (red) or allospecific (green) strains. **c**, Differential regulation of selected operons by simvastatin (purple dots), sertraline (green dots), paroxetine (blue dots) or levothyroxine (red) dots is depicted for different conspecific strains (purple boxes depict operon expression in strain H1; yellow boxes depict operon expression in a publicly available strain). Grey dots indicate $P_{adj} > 0.05$. Species and operon identities are indicated by panel titles, and strain identity is shown on the right *y*-axis. The $\log_2$(FC) in gene expression compared with that of a vehicle control is shown on the left *y*-axis, and aligned gene identities (IDs) are shown on the *x*-axis. The absence of an operon is indicated by a beige panel with red annotation. Grey dashed lines and boxes indicate the significance threshold of FC > 2.

(Fig. 5b). Furthermore, a significant decrease in relative abundance of the *acrAB-tolC* operon ($P_{adj} = 0.0102$) in the gut microbiome of patients receiving simvastatin was observed (Fig. 5b). In contrast, *acrAB-tolC* gene abundance was not changed in patients who received atorvastatin, fluvastatin, pravastatin or rosuvastatin. Accordingly, simvastatin-treated patients also showed a significant depletion in *Bacteroides* species ($P = 0.0030$), as well as increases in *Alistipes* and unclassified Firmicutes (Fig. 5c). Moreover, *Bacteroides* and other bacteria containing a complete AcrAB-TolC homologue were significantly depleted in simvastatin-treated cohorts compared with untreated controls ($P = 0.0013$), whereas bacteria missing this operon were not depleted ($P = 0.699$; Fig. 5d). Notably, a relative abundance analysis for the separate gene components of the *acrAB-tolC* operon in statin-treated cohorts identified the most significant depletion ($P = 0.003$) in the *AcrB2* gene, which encodes a homotrimer docked to the intracellular bacterial membrane that binds to pump substrates (Supplementary Fig. 13)[61].

Taking all these data together, we posit a potential model of statin-mediated depletion of gut microorganisms containing the AcrAB-TolC efflux pump (Supplementary Fig. 14). Under normal conditions, gut microbial residents containing AcrAB-TolC homologues (for example, Bacteroidales species) use this pump to prevent periplasmic and cytoplasmic accumulation of metabolites, such as retinol and deoxycholic acid, to toxic levels. In the context of simvastatin treatment, *acrAB-tolC* is upregulated, leading to increased collateral sensitivity to dietary metabolites and reduced cell viability. Efflux pump upregulation leading to decreased bacterial viability has been observed in clinical cohorts[64], although the mechanism of this phenomenon has not been elucidated to date. Notably, the prototypical *acrAB-tolC* operon is regulated by the self-contained *acrR* repressor (Fig. 3d), which in *Escherichia coli* is strongly upregulated under conditions of global stress[65]. Thus, it is possible that by inducing AcrR expression, engineered AcrAB-TolC pump overexpression could indirectly impact co-regulation of global stress response and lead to reduced cell viability. Regardless, with simvastatin treatment, increased expression of AcrAB-TolC causes decreased viability of gut bacteria and consequential alterations in gut microbiota composition.

Strain differences in drug-mediated transcriptomic responses

Finally, we sought to explore how drug–microorganism transcriptional responses differed among strains in our panel (Fig. 6 and Supplementary Fig. 15). First, we analysed the DEGRs across all drugs by PCoA

to quantify similarities in global transcriptomic profiles of strains. Interestingly, we found that microbial responses to drugs clustered significantly at the family level [that is, Bacteroidaceae, Lachnospiraceae, $P = 0.003$ by permutational multivariate analysis of variance (PERMANOVA) test; Fig. 6a], suggesting that closely related bacteria may respond similarly to different drugs. However, a detailed comparison of conspecific strains revealed a more variable pattern of response. For example, while strains of *A. rectalis* (H1 versus ATCC 33656) exhibited highly consistent drug responses, strains of *B. uniformis* (H1 versus ATCC 8492) responded more heterogeneously to pharmaceuticals (Fig. 6a).

To further delineate the strain specificity of drug responses, we next quantified the average nucleotide similarity (ANI) between different Bacteroidales strain pairs, which we compared with the correlation of global transcriptomic response (DEGR values) between strains (Fig. 6b). We observed higher correlations ($R > 0.7$) in overall drug response between pairs with the greatest ANI values (ANI > 0.95), suggesting that the more similar the bacterial genome, the more similar the global transcriptomic response across drug conditions (Fig. 6b). To compare the transcriptomic responses of conspecific strains more closely, we next aligned the genomes for all conspecific strains (Methods). We observed high correlations ($R^2 > 0.79$) in expression of shared genes between all conspecific strain pairs, suggesting shared transcriptional responses between isolates (Supplementary Fig. 15).

We next sought to investigate strain-level drug response at the operon level. Remarkably, we identified two common types of transcriptional differences between conspecific strains: (1) absence of an operon in one isolate and (2) differential regulation of a shared operon between isolates, with both differences possibly having functional impacts. For example, sertraline upregulated a mobile element containing type IV secretion system machinery in *A. rectalis* H1 that was not present in *A. rectalis* ATCC 33656 (Fig. 6c). Similarly, sertraline and paroxetine upregulated BepE efflux machinery in *B. uniformis* H1 that was not present in ATCC 8492 (Fig. 6c). On the other hand, several drugs (sertraline, paroxetine, levothyroxine, simvastatin) downregulated a shared putative L-arabinose utilization operon in *A. rectalis* H1, but this same operon (98.31% average conservation in coding sequence) was not differentially expressed in *A. rectalis* 33656 (Fig. 6c). Conversely, these compounds downregulated a shared putative transketolase operon (99.89% average conservation in coding sequence) in *A. rectalis* 33656 only (Fig. 6c). Interestingly, in addition to differences in shared operon expression between isolates, we also observed instances of differential regulation of different gene copies by the same drug perturbation (Fig. 6c). For example, within *F. saccharivorans* DSMZ 26062, levothyroxine, sertraline, simvastatin and paroxetine exposures triggered simultaneous upregulation and downregulation of different copies of araQ, a permease protein associated with L-arabinose transport (99.25% average conservation in coding sequence; Fig. 6c). A high degree of strain-level functional diversity could explain the substantial microbiome compositional variation often observed in clinical drug studies that rely on only 16S taxonomic analysis rather than whole genome sequencing. Together, these results underline the importance of assessing bacterial drug responses at the strain level with genomic information, as well as extending traditional microbiota drug screens to multiple conspecific strains to capture the full intra-strain diversity of drug responses.

Discussion

While numerous clinical studies suggest prevalent drug–microbiota interactions[5,13,23,25], genetic-level understanding of xenobiotic-induced microbiota shifts remains limited. In this study, we generated a transcriptome dataset for exploring gut microbiota–drug responses to common orally delivered drugs, totalling >400 bacterial–drug pairwise interactions. With this dataset, we uncovered that simvastatin-mediated upregulation of the AcrAB-TolC efflux pump generates collateral toxicity to dietary metabolites ex vivo. Using a clinical metagenomic dataset, we confirmed that AcrAB-TolC-containing gut bacteria are depleted in patients taking simvastatin, suggesting that upregulation of *acrAB-tolC* under statin exposure increases cellular toxicity.

Beyond statins, our data established clinically relevant links between cardiovascular medications and SSRIs and the gut microbiome. Our ex vivo data and computational analysis of T2D patient data suggest the upregulation of tartrate metabolism in gut microorganisms exposed to metoprolol. This result motivates the need for further clinical studies to determine whether metoprolol tartrate places patients at higher risk of developing T2D and other metabolic disorders. The clinical dataset used in our analysis does not distinguish metoprolol tartrate versus metoprolol succinate, which are used as short- or long-form treatment. As metoprolol tartrate exhibits a greater interindividual variation in bioavailability[44], future work exploring the impact of microbiome metabolism on the in vivo bioavailability of metoprolol tartrate and other tartrate-conjugated pharmaceuticals is warranted. Separately, our findings provide evidence that drugs can modulate riboflavin production by gut bacteria. Mechanistic delineation of how pharmaceuticals induce or repress vitamin B_2 production could enable the development of tools to promote microbial production of this essential vitamin[51]. As vitamin B_2 depletions have been linked to depression and atherosclerosis[52,53,55], our data also motivate clinical studies of whether *rib*-modulating medications impact key vitamin reservoirs in the microbiomes of psychiatric and cardiovascular patients, and whether these interactions impact disease pathology.

From an ecological standpoint, shared transcriptional responses could provide mechanistic insights into how pharmaceuticals drive shifts in microbiome populations over time. Our pathway meta-analysis showed that many drugs upregulate highly conserved bacterial multidrug efflux pumps. Efflux-associated pathways were distinct from resistance pathways upregulated by traditional antibiotics, suggesting novel mechanisms of drug-driven microbiota responses. Our results showing efflux-mediated collateral toxicity induced by simvastatin–retinol co-incubation underline the importance of exploring the molecular efflux networks to identify drug–efflux pump interactions that can result in gut microbiota shifts. Furthermore, recent data have linked chronic prescription drug use and polypharmacy with antimicrobial resistance in gut microbiota[4]. One work even linked the upregulation of efflux pumps by four antidepressants used in our study (sertraline, duloxetine, escitalopram and bupropion) to the promotion of antimicrobial resistance among gut community members[66]. These data all suggest that chronic medication-induced increases in the activity of efflux pumps could contribute to higher rates of antimicrobial resistance among gut microbiota within patient populations.

Our study has several limitations. Ex vivo screens cannot capture the full environmental complexity that may exist between microbiota community members and the host in vivo, and transcriptomics does not directly probe host-mediated drug–microbiota interactions. While many of our observed inhibitory drug activities aligned with published clinical data[5,25], we detected neither growth nor transcriptional changes in gut bacteria exposed to metformin. The role of host-derived factors mediating metformin-induced microbiota shifts is well documented (that is, secondary bile acids cause depletion of *Bacteroides* and enrichment of *Escherichia* species that trigger downstream regulation of the farnesoid receptor)[67]. This and other instances of low transcriptomic signals generated in our study by drugs linked to microbiota changes in vivo (for example, omeprazole) could suggest missing host- or community-derived factors, motivating future in vivo studies that integrate these other factors (for example, bile acids and dietary vitamins). While we leveraged published clinical microbiome data to further validate our ex vivo drug–microorganism interaction results, our simvastatin findings could benefit from prospective clinical trials designed to dissect the impacts of simvastatin and disease status on gut microbiota dynamics, and to determine whether AcrAB-TolC is

simply a biomarker or a functional mediator of simvastatin-associated gut microbiota shifts.

Altogether, this work has shown the utility of high-throughput transcriptomics to delineate microbiota–drug interactions. We envision that this low-cost and scalable pipeline can be easily applied to any microbiota–treatment pairing including xenobiotic, prebiotic and probiotic treatments. These efforts will lead to a greater mechanistic understanding of how different environmental exposures impact the gut microbiome that in turn can affect host health and response to medical interventions.

Methods

Materials and culture conditions

All bacteria used in this study have fully sequenced genomes, the information for which can be found in Supplementary Table 3. Natural bacterial isolates used in this study were derived from a single faecal sample taken from a healthy individual for an unrelated study. The sex and gender of this individual, while reported in the unrelated study, were deemed irrelevant in this study and were not reported. This work was approved and conducted under Columbia University Medical Center Institutional Review Board protocol AAAR0753, and written informed consent was obtained from the subject. Additional conspecific strains of *A. rectalis*, *F. saccharivorans*, *B. uniformis*, *P. vulgatus* and *B. fragilis*, as well as the *Eggerthella lenta* strain described in ref. 15, were obtained from public strain catalogues. All publicly available strains used in this study were purchased either from the American Type Culture Collection or from the Leibniz Institute DSMZ-German Collection of Microorganisms and Cell Cultures GmbH. All monoclonal isolates were Sanger sequenced (Azenta Life Sciences) at the 16Sv4 region pre- and post-experimentation to confirm strain identity. Natural isolates used in this study are available from the corresponding author upon request.

For our drug panel, we selected 19 orally administered drugs from the top-prescribed pharmaceuticals in 2017 according to the Agency for Healthcare Research and Quality (Supplementary Table 4)[31]. This list included the top eight most prescribed drugs, included lisinopril, atorvastatin, levothyroxine, metformin, amlodipine, metoprolol, omeprazole and simvastatin. Additional neurotransmitter modulators were selected from the top 25 drugs prescribed, as follows: sertraline, fluoxetine, citalopram, escitalopram, paroxetine, duloxetine, venlafaxine, amitriptyline, bupropion and trazodone. We finally included lenalidomide owing to its large market cap[31]. All chemicals used in this study were purchased from Sigma-Aldrich, Thermo Scientific Chemicals or Avantor (Supplementary Tables 4, 9 and 10). Probes for rRNA depletions were purchased from Integrated DNA Technologies. Unless otherwise noted, bacterial cultures were grown in one-half-diluted Gifu Anaerobic Medium Broth, Modified (mGAM, HyServe 05433) media prepared according to manufacturers' instructions. Before experimentation, all mGAM media were reduced for 24 h under anaerobic conditions (5% H_2, 10% CO_2, 85% N_2) within a Coy Laboratory Products anaerobic chamber. Chemical plates were prepared in 96-well format under aerobic sterile conditions and reduced for 3–6 h before experimentation.

Bacterial transcriptome preparation and extraction

For all transcriptomic experiments, bacterial cultures at exponential phase were added to 96-deep-well plates (Axygen P-DW-20-C) containing pre-reduced chemicals to reach a final concentration of 20 µM (500 µM for metformin). After 90 min of exposure in shaken media at 37 °C, cultures were centrifuged, the supernatant was removed and cell pellets were transferred to −80 °C before bacterial RNA extraction.

Bacterial RNA was extracted using RNAsnap methods[68]. Briefly, frozen bacterial pellets were suspended in 500 µl RNAsnap mix (95% formamide, 18 mM ethylenediaminetetraacetic acid, 0.025% sodium dodecyl sulphate, 1% B-mercaptoethanol) before addition of ~200 µl of 0.1 mm zirconia silica beads (Biospec 11079101Z). Cells were then lysed by bead beating for 3 × 2.5 min in a Biospec Mini Bead Beater (Biospec 1001) with 5-min intervals and then subjected to centrifugation at 4,300 × *g* for 5 min. The clean supernatant was then transferred to a new deep-well plate, and RNA was purified using a Zymo ZR-96 RNA Clean & Concentrator Kit (Zymo R1080) per manufacturer's instructions.

RNA-seq library preparation and sequencing

RNA-seq libraries were constructed following a modified RNAtag-seq protocol as detailed in ref. 24. Briefly, 400 ng of total RNA lysate was subjected to fragmentation in 2× FastAP buffer (ThermoFisher EF0651), genomic DNA removal (TURBO DNase, ThermoFisher AM2239) and dephosphorylation (FastAP, ThermoFisher EF0651). Fragmented RNA was purified using SeraPure SPRI bead cleanup[69] and ligated with barcoded first adapter ligation by T4 RNA ligase I (NEB M0437M). After pooling and purification with the Zymo RNA Clean & Concentrator-5 Kit (Zymo R1015), we quantified barcoded RNA using a Qubit RNA HS Assay Kit (ThermoFisher Q32855) and then performed RNase-H-based ribosomal RNA depletion on 400 ng of barcoded RNA sample using a 10:1 probe-to-RNA ratio, as previously outlined[24].

rRNA-depleted RNA was subjected to downstream library preparation following standard RNAtag-seq protocols[27], including reverse transcription (ThermoFisher 18090010) and second adapter ligation (NEB M0437M). Ligation products were further amplified with primers containing Illumina P5 and P7 adapters and sample indexes, and polymerase chain reactions (PCRs) were stopped during exponential amplification. PCR products were subjected to gel electrophoresis on E-Gel EX Agarose Gels, 2% (ThermoFisher G402002) and expected DNA smears (300–600 bp) were excised and extracted using the Monarch DNA Gel Extraction Kit (NEB T1020L). Resulting libraries were sequenced to a minimum of 4.9× (Supplementary Table 6). Sequences of all adapters and primers used in library preparation are provided in ref. 24.

RNA-seq data analyses

RNA libraries were analysed for differential expression analysis as outlined in ref. 24, which lists all adapter and primer sequences used. Briefly, raw sequencing reads were demultiplexed using Sabre[70] and bcl2fastq[71] before adapter removal with Cutadapt v2.1 (ref. 72), using parameters '-a file:[RNAtagSeq adapter.fa] -u 5 –minimum-length 20 –max-n 0 -q 20' to remove low-quality bases and adapters. To mitigate the effect of rRNA reads, we performed alignments against the 16S and 23S rRNAs of corresponding strains with Bowtie2 (ref. 73), using the versions and parameters outlined in ref. 24. Genomes of natural isolates used for sequencing alignments were de novo assembled as described in ref. 24. Genome assemblies for all publicly available isolates were downloaded from the NCBI database, with all accession numbers listed in Supplementary Table 3. The number of reads uniquely mapped to each coding sequence was calculated using featureCounts v1.6.2 (ref. 74) without restraint on strandness (-s 0), and the expression level of each coding sequence (CDS) by transcripts per million (TPM) was quantified using an in-house script.

Finally, we used DESeq2 (ref. 75) to perform differential expression analysis on the number of reads uniquely mapped to each coding sequence, calculating the FC of gene expression after perturbations. Differential gene expression was defined as >2 FC in gene expression relative to a vehicle control, with $P_{adj} < 0.05$, and average fragments per kilobase per million reads aligning to annotated open reading frame (FPKMO) > 0.10. *P* values of differential expression were all adjusted using the Benjamini–Hochberg procedure in DESeq2 using default settings. Identified DEGs were used to identify drug-enriched modules and pathways using the KEGG database[76]. KEGG enrichment with $P_{adj} < 0.05$ and $e < .00001$ was considered statistically significant. All analyses were visualized in R[77].

Growth assays

For all growth experiments, overnight bacterial cultures were back diluted 1:100 before addition to 96-well plates containing 5–25 µl of pre-reduced chemicals or bile acids to reach 2, 20 or 100 µM concentrations in 1 ml of solution (all concentrations for bacterial–drug pairings are listed in Supplementary Fig. 2). As an exception, higher concentrations of 50, 500 and 2,500 µM were used for metformin (Methods and Supplementary Fig. 2), which has much higher predicted drug concentrations in the intestinal tract[5]. Furthermore, *A. shahii* was not included in growth experiments as it exhibits characteristically poor growth in liquid that prevents optical density measurements[78]. Cultures were then incubated at 37 °C in shaken media for 24 h. For 24 h temporal growth screens, 190 µl of culture was collected at 6, 10 and 24 h for measurement of OD_{600} using an Epoch2 Microplate Spectrophotometer (Agilent Technologies). For all MIC tests, cultures were collected for visual inspection and OD_{600} measurement at 24 h only. Growth inhibition was defined in all growth experiments as relative growth depletion >30%, with false discovery rate (FDR)-adjusted *P* value (P_{adj}) < 0.05. To determine statistical differences in relative growth between conditions, two-sided independent *t*-tests with Benjamini–Hochberg correction were performed in R to determine FDR-adjusted *P* values unless otherwise stated.

Analysis of public datasets

To identify species harbouring the *acrAB-tolC* operon, we generated an amino acid reference from the *P. vulgatus acrAB-tolC* operon detailed in ref. 57. We then performed a homologue search for this reference operon in a public dataset of 4,930 representative MAGs characterized in ref. 63. Briefly, we annotated all putative protein sequences in the MAG dataset using Prokka[79] before performing a homologue search with blastP[80]. Gene targets with an *e* value < 10^{-5}, coverage > 90% and identity > 40% were considered hits. We then estimated abundances of all species containing the *acrAB-tolC* operon using metadata from ref. 63. All associated *P* values were calculated using the two-tailed independent *t*-test in R.

To examine whether metoprolol administration could be linked to the upregulation of the *ttd* operon in vivo, raw amplicon sequencing data from a public dataset ($n = 145$) were downloaded from Sequence Read Archive under accession code ERP002469. Single-ended raw reads were processed by Cutadapt v2.1 (ref. 72) with the following parameters '–minimum-length 24 -u 10–trim-n -q 15' to remove low-quality bases and Illumina adapters. Reads passing quality filtering were then aligned against our *ttd* operon reference by Bowtie2 v2.3.4 (ref. 73) in very-sensitive mode. Read counts per gene were normalized by gene length and sequencing depth (that is, reads per kilobase per million mapped reads) for expression-level quantification. All associated *P* values were calculated using the Mann–Whitney test in R.

To examine whether simvastatin-modulated microbiota shifts could be linked to *acrAB-tolC* operon prevalence in vivo, raw amplicon sequencing data from the cross-sectional MetaCardis BMIS cohort ($n = 888$) were downloaded from the EMBL-EBI European Nucleotide Archive under accession number PRJEB37249. Single-ended raw reads were processed by Cutadapt v2.1 (ref. 72) with the following parameters '–minimum-length 24 -u 10–trim-n -q 15' to remove low-quality bases and Illumina adapters. Reads passing quality filtering were then aligned against our *acrAB-tolC* operon reference by Bowtie2 v2.3.4 (ref. 73) in very-sensitive mode. Read counts per gene were normalized by gene length and sequencing depth (that is, reads per kilobase per million mapped reads) for expression-level quantification. All associated *P* values were calculated using the two-tailed independent *t*-test in R.

AcrAB-TolC Engineering Studies

All *Bacteroides* expression vectors were generated using Gibson assembly (NEBuilder 2x HiFi DNA assembly master mix), and PCR fragments for cloning were generated using Q5 DNA Polymerase (NEB). We first generated two PCR fragments from a plasmid designed and constructed in our laboratory containing constitutive Bacteroidales promoters described in ref. 81 (additional features of this custom vector backbone are described in a separate manuscript currently under consideration) to drive expression of the AcrAB-TolC gene copies. We then cloned AcrAB-TolC copy 1 (primers TCTCGTCAAACAAATATAAATAATATAAACATGAAAATGACAGTAAATAGTATGAAATGT and AGAAGGGCACCAATAACTGCCTTAAAAAAATTAATTATTCACGTCCACCGC) and copy 2 (primers TCTCGTCAAACAAATATAAATAATATAAACATGAAATTTTATTGCAAACCTACGT and AGAAGGGCACCAATAACTGCCTTAAAAAAATTATTCTTTTTTGCCTTTGGTCATC) from the *P. vulgatus* H1 genome using PCR. A three-fragment Gibson assembly was incubated at 50 °C for 1 h to generate our plasmid construct. As a control, we cloned a tetracycline (Tet)-resistance gene (described in ref. 82) into our plasmid construct in place of AcrAB-TolC cargo. Finally, AcrAB-TolC-containing plasmids (or Tet plasmid controls) were transformed into chemically competent NEB turbo cells. Transformed colonies were screened by PCR for the correct insert size length, and whole plasmids were sequenced on an Illumina NextSeq 500/550 platform or using Plasmidsaurus. Vector constructs with the correct payload were used in subsequent conjugation experiments.

Before conjugation, donor strains harbouring conjugative *Bacteroides* expression vectors were grown from a single colony in 5 ml of LB-Lennox media (BD) supplemented with 50 µg ml^{-1} of carbenicillin and 50 µM DAP at 37 °C overnight (~10–16 h). We prepared donor and recipient *P. vulgatus* H1 cells and carried out conjugations as previously described in ref. 83 under anaerobic conditions. Transconjugant colonies were Sanger sequenced at the 16Sv4 region to confirm strain identity, and stable plasmid maintenance was confirmed with colony PCR using the primers listed above. Positive *P. vulgatus* transconjugants were then picked into 5 ml one-half mGAM supplemented with 20 µg ml^{-1} erythromycin and grown overnight. These strains were banked in glycerol stocks (25% glycerol final concentration) and stored at −80 °C. Subsequent growth curve experiments were done using overnight cultures grown from these glycerol stocks in one-half mGAM.

Conspecific strain gene mapping

To compare the transcriptomic response for strains of the same species, we performed gene mapping for five pairs of conspecific strains used in this study. Briefly, all protein sequences of the strains were first annotated using Prokka[79]. Protein alignment was then performed for the protein sequences of conspecific strains by blastP[80] using the parameters '-max_target_seqs 20 -evalue 0.001'. Hits with identity >0.75 and coverage >0.75 were considered as mapped genes for conspecific strains.

Statistics and reproducibility

For all isolates generated in this study, individual origins of isolated gut strains were assigned based on the defined identity of original faeces (Supplementary Table 2), for which covariate analysis is not applicable. The specific number of bacterial strains used in this study (19) was chosen to allow for inclusion of major bacterial phyla within an individual donor microbiome, with replicates included as described in Methods to allow for statistical significance calculations. For clinical datasets analysed, the cohort assignment for individuals was taken from the metadata of the original study. Blinding was not possible during experiments as we were comparing transcriptional responses of different bacterial isolates to different drug conditions. Transcriptomic and growth processing within species was blinded as different drug conditions were processed together using pooled methods. Data exclusion was based on sequencing coverage or genome quality to remove technical artifacts as described in Methods. The sample sizes in this study are either number of bacterial strains tested (with replicates; see below) or number of experimental or control

cohort individuals taken from a publicly available dataset (for which sample size calculations were already performed). All sample sizes are listed in figure legends and Methods sections where applicable. All in vitro assays on bacterial strains were performed with multiple (two to four) technical replicates, as noted in Methods and figure legends where applicable, to confirm replicability and enable statistical significance calculations. All analyses of associated data were performed with the same parameters and criteria described in Methods. Data distribution was assumed to be normal, but this was not formally tested.

Reporting summary

Further information on research design is available in the Nature Portfolio Reporting Summary linked to this article.

Data availability

All sequencing data generated in this study have been submitted to the NCBI BioProject database (http://www.ncbi.nlm.nih.gov/bioproject/) under accession number PRJNA925551.

Code availability

Scripts used to analyse sequencing data in this study can be accessed at https://github.com/wanglabcumc/microbial_RNAseq_processing.

References

1. *Global Medicine Spending and Usage Trends: Outlook to 2025* (IQVIA Institute, 2021).
2. *Health, United States 2019* (National Center for Health Statistics, accessed 14 October 2022); https://www.cdc.gov/nchs/hus/contents2019.htm#Table-039
3. Sonnenburg, J. L. & Sonnenburg, E. D. Vulnerability of the industrialized microbiota. *Science* **366**, eaaw9255 (2019).
4. Nagata, N. et al. Population-level metagenomics uncovers distinct effects of multiple medications on the human gut microbiome. *Gastroenterology* **163**, 1038–1052 (2022).
5. Maier, L. et al. Extensive impact of non-antibiotic drugs on human gut bacteria. *Nature* **555**, 623–628 (2018).
6. Jackson, M. A. et al. Proton pump inhibitors alter the composition of the gut microbiota. *Gut* **65**, 749–756 (2016).
7. *National Ambulatory Medical Care Survey: 2018 National Summary Tables* (National Center for Health Statistics, 2018).
8. Singh, R. et al. Enhancement of the gut barrier integrity by a microbial metabolite through the Nrf2 pathway. *Nat. Commun.* **10**, 89 (2019).
9. Roager, H. M. et al. Colonic transit time is related to bacterial metabolism and mucosal turnover in the gut. *Nat. Microbiol.* **1**, 16093 (2016).
10. Wexler, A. G. et al. Human gut *Bacteroides* capture vitamin B_{12} via cell surface-exposed lipoproteins. *eLife* **7**, e37138 (2018).
11. Gopalakrishnan, V., Helmink, B. A., Spencer, C. N., Reuben, A. & Wargo, J. A. The influence of the gut microbiome on cancer, immunity, and cancer immunotherapy. *Cancer Cell* **33**, 570–580 (2018).
12. Porras, A. M. et al. Inflammatory bowel disease-associated gut commensals degrade components of the extracellular matrix. *mBio* **13**, e02201–e02222 (2022).
13. Gopalakrishnan, V. et al. Gut microbiome modulates response to anti-PD-1 immunotherapy in melanoma patients. *Science* **359**, 97–103 (2018).
14. Khoruts, A. & Sadowsky, M. J. Understanding the mechanisms of faecal microbiota transplantation. *Nat. Rev. Gastroenterol. Hepatol.* **13**, 508–516 (2016).
15. Haiser, H. J. et al. Predicting and manipulating cardiac drug inactivation by the human gut bacterium *Eggerthella lenta*. *Science* **341**, 295–298 (2013).
16. Heinken, A. et al. Genome-scale metabolic reconstruction of 7,302 human microorganisms for personalized medicine. *Nat. Biotechnol.* **41**, 1320–1331 (2023).
17. Zimmermann, M., Zimmermann-Kogadeeva, M., Wegmann, R. & Goodman, A. L. Separating host and microbiome contributions to drug pharmacokinetics and toxicity. *Science* **363**, eaat9931 (2019).
18. Takasuna, K. et al. Involvement of beta-glucuronidase in intestinal microflora in the intestinal toxicity of the antitumor camptothecin derivative irinotecan hydrochloride (CPT-11) in rats. *Cancer Res.* **56**, 3752–3757 (1996).
19. Klünemann, M. et al. Bioaccumulation of therapeutic drugs by human gut bacteria. *Nature* **597**, 533–538 (2021).
20. Zhang, Y. et al. Metatranscriptomics for the human microbiome and microbial community functional profiling. *Annu. Rev. Biomed. Data Sci.* **4**, 279–311 (2021).
21. Lloréns-Rico, V., Simcock, J. A., Huys, G. R. B. & Raes, J. Single-cell approaches in human microbiome research. *Cell* **185**, 2725–2738 (2022).
22. Spanogiannopoulos, P. et al. Host and gut bacteria share metabolic pathways for anti-cancer drug metabolism. *Nat. Microbiol.* **7**, 1605–1620 (2022).
23. Rekdal, V. M., Bess, E. N., Bisanz, J. E., Turnbaugh, P. J. & Balskus, E. P. Discovery and inhibition of an interspecies gut bacterial pathway for levodopa metabolism. *Science* **364**, eaau6323 (2019).
24. Huang, Y., Sheth, R. U., Kaufman, A. & Wang, H. H. Scalable and cost-effective ribonuclease-based rRNA depletion for transcriptomics. *Nucleic Acids Res.* **48**, E20 (2020).
25. Vieira-Silva, S. et al. Statin therapy is associated with lower prevalence of gut microbiota dysbiosis. *Nature* **581**, 310–315 (2020).
26. Fuentes, A. V., Pineda, M. D. & Venkata, K. C. N. Comprehension of top 200 prescribed drugs in the US as a resource for pharmacy teaching, training and practice. *Pharmacy* **6**, 43 (2018).
27. Shishkin, A. A. et al. Simultaneous generation of many RNA-seq libraries in a single reaction. *Nat. Methods* **12**, 323–325 (2015).
28. Turnbaugh, P. J. et al. The Human Microbiome Project. *Nature* **449**, 804–810 (2007).
29. Derrien, M., Turroni, F., Ventura, M. & van Sinderen, D. Insights into endogenous *Bifidobacterium* species in the human gut microbiota during adulthood. *Trends Microbiol.* **30**, 940–947 (2022).
30. Martinson, J. N. V. & Walk, S. T. *Escherichia coli* residency in the gut of healthy human adults. *EcoSal Plus* https://doi.org/10.1128/ECOSALPLUS.ESP-0003-2020 (2020).
31. Kane, S. P. *The Top 300 of 2017. ClinCalc Drugstats Database* (ClinCalc LLC, 2021).
32. Goh, E. B. et al. Transcriptional modulation of bacterial gene expression by subinhibitory concentrations of antibiotics. *Proc. Natl Acad. Sci. USA* **99**, 17025–17030 (2002).
33. Gibson, B., Wilson, D. J., Feil, E. & Eyre-Walker, A. The distribution of bacterial doubling times in the wild. *Proc. R. Soc. B* **285**, 20180789 (2018).
34. Zhu, Z. et al. Entropy of a bacterial stress response is a generalizable predictor for fitness and antibiotic sensitivity. *Nat. Commun.* **11**, 4365 (2020).
35. Vicente, M., Chater, K. F. & De Lorenzo, V. Bacterial transcription factors involved in global regulation. *Mol. Microbiol.* **33**, 8–17 (1999).
36. Cayres, L. C. et al. Detection of alterations in the gut microbiota and intestinal permeability in patients with Hashimoto thyroiditis. *Front. Immunol.* **12**, 579140 (2021).
37. Bajaj, J. S. et al. Posttraumatic stress disorder is associated with altered gut microbiota that modulates cognitive performance in veterans with cirrhosis. *Am. J. Physiol. Gastrointest. Liver Physiol.* **317**, G661 (2019).

38. Poole, K. Efflux-mediated multiresistance in Gram-negative bacteria. *Clin. Microbiol. Infect.* **10**, 12–26 (2004).
39. Du, D. et al. Multidrug efflux pumps: structure, function and regulation. *Nat. Rev. Microbiol.* **16**, 523–539 (2018).
40. Sun, J., Deng, Z. & Yan, A. Bacterial multidrug efflux pumps: mechanisms, physiology and pharmacological exploitations. *Biochem. Biophys. Res. Commun.* **453**, 254–267 (2014).
41. Bryan, L. E., Kowand, S. K. & Van Den Elzen, H. M. Mechanism of aminoglycoside antibiotic resistance in anaerobic bacteria: *Clostridium perfringens* and *Bacteroides fragilis*. *Antimicrob. Agents Chemother.* **15**, 7–13 (1979).
42. Zimmermann, M., Zimmermann-Kogadeeva, M., Wegmann, R. & Goodman, A. L. Mapping human microbiome drug metabolism by gut bacteria and their genes. *Nature* **570**, 462–467 (2019).
43. Gruetter, C. in *xPharm: The Comprehensive Pharmacology Reference* 1–7 (Elsevier, 2007); https://doi.org/10.1016/B978-008055232-3.62174-9
44. Sandberg, A., Blomqvist, I., Jonsson, U. E. & Lundborg, P. Pharmacokinetic and pharmacodynamic properties of a new controlled-release formulation of metoprolol: a comparison with conventional tablets. *Eur. J. Clin. Pharmacol.* **33**, S9–S14 (1988).
45. Kohn, L. D. & Jakoby, W. B. Tartaric acid metabolism: III. The formation of glyceric acid. *J. Biol. Chem.* **243**, 2465–2471 (1968).
46. Sobiecka, A., Synoradzki, L., Hajmowicz, H. & Zawada, K. Tartaric acid and its derivatives. Part 17. Synthesis and applications of tartrates. *Org. Prep. Proced. Int.* **49**, 1–27 (2017).
47. Proffitt, C. et al. Genome-scale metabolic modelling of the human gut microbiome reveals changes in the glyoxylate and dicarboxylate metabolism in metabolic disorders. *iScience* **25**, 104513 (2022).
48. Cai, L., Wu, H., Li, D., Zhou, K. & Zou, F. Type 2 diabetes biomarkers of human gut microbiota selected via iterative sure independent screening method. *PLoS ONE* **10**, e0140827 (2015).
49. Fuchs, F. D. & Whelton, P. K. High blood pressure and cardiovascular disease. *Hypertension* **75**, 285–292 (2020).
50. Yoshii, K., Hosomi, K., Sawane, K. & Kunisawa, J. Metabolism of dietary and microbial vitamin B family in the regulation of host immunity. *Front. Nutr.* **6**, 48 (2019).
51. Averianova, L. A., Balabanova, L. A., Son, O. M., Podvolotskaya, A. B. & Tekutyeva, L. A. Production of vitamin B_2 (riboflavin) by microorganisms: an overview. *Front. Bioeng. Biotechnol.* **8**, 1172 (2020).
52. Wu, Y., Zhang, L., Li, S. & Zhang, D. Associations of dietary vitamin B_1, vitamin B_2, vitamin B_6, and vitamin B_{12} with the risk of depression: a systematic review and meta-analysis. *Nutr. Rev.* **80**, 351–366 (2022).
53. Rouhani, P. et al. Dietary riboflavin intake in relation to psychological disorders in Iranian adults: an observational study. *Sci. Rep.* **13**, 5152 (2023).
54. García-Minguillán, C. J. et al. Riboflavin status modifies the effects of methylenetetrahydrofolate reductase (MTHFR) and methionine synthase reductase (MTRR) polymorphisms on homocysteine. *Genes Nutr.* **9**, 435 (2014).
55. Gebbers, J. O. Atherosclerosis, cholesterol, nutrition, and statins—a critical review. *Ger. Med. Sci.* **5**, Doc04 (2007).
56. Okusu, H., Ma, D. & Nikaido, H. AcrAB efflux pump plays a major role in the antibiotic resistance phenotype of *Escherichia coli* multiple-antibiotic-resistance (Mar) mutants. *J. Bacteriol.* **178**, 306 (1996).
57. Hibberd, M. C. et al. The effects of micronutrient deficiencies on bacterial species from the human gut microbiota. *Sci. Transl. Med.* https://doi.org/10.1126/SCITRANSLMED.AAL4069 (2017).
58. Ko, H. H. T., Lareu, R. R., Dix, B. R. & Hughes, J. D. Statins: antimicrobial resistance breakers or makers? *PeerJ* **5**, e3952 (2017).
59. Keating, N. et al. Physiological concentrations of bile acids down-regulate agonist induced secretion in colonic epithelial cells. *J. Cell. Mol. Med.* **13**, 2293–2303 (2009).
60. Lenz, K. D., Klosterman, K. E., Mukundan, H. & Kubicek-Sutherland, J. Z. Macrolides: from toxins to therapeutics. *Toxins* **13**, 347 (2021).
61. Jang, S. AcrAB–TolC, a major efflux pump in Gram negative bacteria: toward understanding its operation mechanism. *BMB Rep.* **56**, 326–334 (2023).
62. Nikaido, H., Basina, M., Nguyen, V. & Rosenberg, E. Y. Multidrug efflux pump AcrAB of *Salmonella typhimurium* excretes only those β-lactam antibiotics containing lipophilic side chains. *J. Bacteriol.* **180**, 4686–4692 (1998).
63. Pasolli, E. et al. Extensive unexplored human microbiome diversity revealed by over 150,000 genomes from metagenomes spanning age, geography, and lifestyle. *Cell* **176**, 649–662.e20 (2019).
64. Imamovic, L. et al. Drug-driven phenotypic convergence supports rational treatment strategies of chronic infections. *Cell* **172**, 121–134.e14 (2018).
65. Ma, D., Alberti, M., Lynch, C., Nikaido, H. & Hearst, J. E. The local repressor AcrR plays a modulating role in the regulation of acrAB genes of *Escherichia coli* by global stress signals. *Mol. Microbiol.* **19**, 101–112 (1996).
66. Wang, Y. et al. Antidepressants can induce mutation and enhance persistence toward multiple antibiotics. *Proc. Natl Acad. Sci. USA* **120**, e2208344120 (2023).
67. Lien, F. et al. Metformin interferes with bile acid homeostasis through AMPK-FXR crosstalk. *J. Clin. Invest.* **124**, 1037–1051 (2014).
68. Stead, M. B. et al. RNAsnap™: a rapid, quantitative and inexpensive, method for isolating total RNA from bacteria. *Nucleic Acids Res.* **40**, e156 (2012).
69. Rohland, N. & Reich, D. Cost-effective, high-throughput DNA sequencing libraries for multiplexed target capture. *Genome Res.* **22**, 939–946 (2012).
70. sabre—a barcode demultiplexing and trimming tool for FastQ files. *GitHub* https://github.com/najoshi/sabre (2022).
71. bcl2fastq conversion user guide (Illumina, 2013).
72. Martin, M. Cutadapt removes adapter sequences from high-throughput sequencing reads. *EMBnet. J.* **17**, 10–12 (2011).
73. Langmead, B. & Salzberg, S. L. Fast gapped-read alignment with Bowtie 2. *Nat. Methods* **9**, 357–359 (2012).
74. Liao, Y., Smyth, G. K. & Shi, W. FeatureCounts: an efficient general purpose program for assigning sequence reads to genomic features. *Bioinformatics* **30**, 923–930 (2014).
75. Love, M. I., Huber, W. & Anders, S. Moderated estimation of fold change and dispersion for RNA-seq data with DESeq2. *Genome Biol.* **15**, 550 (2014).
76. Kanehisa, M. & Goto, S. KEGG: Kyoto Encyclopedia of Genes and Genomes. *Nucleic Acids Res.* **28**, 27–30 (2000).
77. Andy Bunn, M. K. A language and environment for statistical computing. *R. Found. Stat. Comput* **10**, 11–18 (2017).
78. Parker, B. J., Wearsch, P. A., Veloo, A. C. M. & Rodriguez-Palacios A. The genus *Alistipes*: gut bacteria with emerging implications to inflammation, cancer, and mental health. *Front. Immunol.* **11**, 906 (2020).
79. Seemann, T. Prokka: rapid prokaryotic genome annotation. *Bioinformatics* **30**, 2068–2069 (2014).
80. Altschul, S. F., Gish, W., Miller, W., Myers, E. W. & Lipman, D. J. Basic local alignment search tool. *J. Mol. Biol.* **215**, 403–410 (1990).
81. Mimee, M., Tucker, A. C., Voigt, C. A. & Lu, T. K. Programming a human commensal bacterium, *Bacteroides thetaiotaomicron*, to sense and respond to stimuli in the murine gut microbiota. *Cell Syst.* **29**, 62–71 (2015).

82. Jeters, R. T., Wang, G. R., Moon, K., Shoemaker, N. B. & Salyers, A. A. Tetracycline-associated transcriptional regulation of transfer genes of the *Bacteroides* conjugative transposon CTnDOT. *J. Bacteriol.* **191**, 6374–6382 (2009).
83. Gelsinger, D. R. et al. Bacterial genome engineering using CRISPR RNA-guided transposases. Preprint at *bioRxiv* https://doi.org/10.1101/2023.03.18.533263 (2023).

Acknowledgements

We thank members of the Wang laboratory for advice and comments on the paper. H.H.W. acknowledges relevant funding support from the NSF (MCB-2025515), NIH (2R01AI132403, 1R01DK118044, 1R01CA272898, 1R01EB031935, 1R21AI146817), ONR (N00014-18-1-2237, N00014-17-1-2353), AFRL (S-168-4X5-001), Burroughs Wellcome Fund (1016691), Irma T. Hirschl Trust and Schaefer Research Award. D.R. acknowledges relevant funding support from the Columbia Medical Scientist Training Program. R.U.S. was supported by a Fannie and John Hertz Foundation Fellowship and an NSF Graduate Research Fellowship (DGE-1644869). D.R.G. was supported by the Burroughs Wellcome Fund Postdoctoral Diversity Enrichment Program.

Author contributions

D.R., Y.H., R.U.S. and H.H.W. developed the initial concepts. D.R. and Y.H. performed experiments and analysed data with assistance from A.K., D.R.G. and R.U.S. and input from H.H.W. D.R., Y.H. and H.H.W. wrote the paper. All other authors discussed results and approved the paper.

Competing interests

H.H.W. is a scientific advisor of SNIPR Biome, Kingdom Supercultures, Fitbiomics, Arranta Bio, VecX Biomedicines and Genus PLC, and a scientific co-founder of Aclid, all of which are not involved in the study. R.U.S is a co-founder of Kingdom Supercultures. Y.H. and H.H.W. are cofounders of Foli Bio. The other authors declare no competing interests.

Additional information

Supplementary information The online version contains supplementary material available at https://doi.org/10.1038/s41564-023-01581-x.

Correspondence and requests for materials should be addressed to Harris H. Wang.

Peer review information *Nature Microbiology* thanks Lisa Maier, Guy Townsend, Tobias Wenzel and the other, anonymous, reviewer(s) for their contribution to the peer review of this work.

nature portfolio

Corresponding author(s): Harris Wang

Last updated by author(s): Aug 31, 2023

Reporting Summary

Nature Portfolio wishes to improve the reproducibility of the work that we publish. This form provides structure for consistency and transparency in reporting. For further information on Nature Portfolio policies, see our Editorial Policies and the Editorial Policy Checklist.

Statistics

For all statistical analyses, confirm that the following items are present in the figure legend, table legend, main text, or Methods section.

n/a	Confirmed	
☐	☒	The exact sample size (*n*) for each experimental group/condition, given as a discrete number and unit of measurement
☐	☒	A statement on whether measurements were taken from distinct samples or whether the same sample was measured repeatedly
☐	☒	The statistical test(s) used AND whether they are one- or two-sided *Only common tests should be described solely by name; describe more complex techniques in the Methods section.*
☐	☒	A description of all covariates tested
☐	☒	A description of any assumptions or corrections, such as tests of normality and adjustment for multiple comparisons
☐	☒	A full description of the statistical parameters including central tendency (e.g. means) or other basic estimates (e.g. regression coefficient) AND variation (e.g. standard deviation) or associated estimates of uncertainty (e.g. confidence intervals)
☐	☒	For null hypothesis testing, the test statistic (e.g. *F*, *t*, *r*) with confidence intervals, effect sizes, degrees of freedom and *P* value noted *Give P values as exact values whenever suitable.*
☒	☐	For Bayesian analysis, information on the choice of priors and Markov chain Monte Carlo settings
☒	☐	For hierarchical and complex designs, identification of the appropriate level for tests and full reporting of outcomes
☐	☒	Estimates of effect sizes (e.g. Cohen's *d*, Pearson's *r*), indicating how they were calculated

Our web collection on statistics for biologists contains articles on many of the points above.

Software and code

Policy information about availability of computer code

Data collection	Illumina sequencing data was collected with MiSeq or NextSeq Software. Growth data was collected with a BioTek Epoch2 Microplate Spectrophotometer using BioTek Gen5 software.

Data analysis	Raw reads of 16SV4 amplicon were analyzed by USEARCH v11.0.667; Taxonomy of OTUs were assigned using Ribosomal Database Project classifier v2.13; Multi-sequence alignment was performed on OTU sequences using MUSCLE v5 and analyzed by MEGA v11.0.11 to calculate phylogeny reconstruction. Raw sequencing reads for transcriptomics experiments were demultiplexed using Sabre and bcl2fastq prior to adapter removal with Cutadapt v2.1 and rRNA alignment using Bowtie2; the number of reads uniquely mapped to each coding sequence was calculated using feature-Counts v1.6.2, and differential expression analysis was done using DESeq2. Bacterial pathways enriched by drug perturbations were identified using the Kyoto Encyclopedia of Genes and Genomes (KEGG) database. For conspecific strain comparison, all protein sequences were annotated using Prokka and protein alignment was performed using Blastp. The average nucleotide identity (ANI) between genomes were calculated by FastANI v1.0. For analysis of all public datasets, raw amplicon sequencing data were downloaded from Sequence Read Archive (SRA) using the cited accession codes. Single-ended raw reads were processed by Cutadapt v2.1. Reads passing quality filtering were then aligned using Bowtie2 v2.3.47. Raw reads for whole-genome sequencing were processed by Cutadapt v2.1 and assembled by Unicycler v0.4.4; The quality and taxonomy of draft genomes were assessed by QUAST v4.6.3, CheckM v1.0.13 and GTDB-Tk v0.2.2; Processed Illumina reads were aligned by Bowtie2 v2.3.4 and alignments were processed by SAMtools v1.9 and BCFtools v1.9 to call genomic variation.

For manuscripts utilizing custom algorithms or software that are central to the research but not yet described in published literature, software must be made available to editors and reviewers. We strongly encourage code deposition in a community repository (e.g. GitHub). See the Nature Portfolio guidelines for submitting code & software for further information.

Data

Policy information about availability of data

All manuscripts must include a data availability statement. This statement should provide the following information, where applicable:

- Accession codes, unique identifiers, or web links for publicly available datasets
- A description of any restrictions on data availability
- For clinical datasets or third party data, please ensure that the statement adheres to our policy

The sequencing data generated in this study have been submitted to the NCBI BioProject database (http://www.ncbi.nlm.nih.gov/bioproject/) under accession number PRJNA925551.

Human research participants

Policy information about studies involving human research participants and Sex and Gender in Research.

Reporting on sex and gender	Bacterial isolates were all isolated from a single healthy individual recruited for an unrelated human research study . Sex and gender of this individual, while reported in the unrelated study, were deemed irrelevant in this study and were not reported.
Population characteristics	All natural bacterial isolates used in this study were derived from a single fecal sample taken from a healthy individual for an unrelated study.
Recruitment	For the unrelated study, healthy volunteers were verbally recruited from Columbia University Medical Center. Exclusion criteria were antibiotic exposure in the last 90 days or active gastrointestinal disease (self-reported), designed to minimize risk of self-selection. Due to the recruitment population, the donors could have been biased towards an age of 20 to 50. Given the exclusion criteria of healthy individuals without antibiotic use, we do not anticipate that the age or characteristics of the individual donor associated with this study impacted the transcriptomics results described.
Ethics oversight	This work was approved and conducted under Columbia University Medical Center Institutional Review Board protocol AAAR0753.

Note that full information on the approval of the study protocol must also be provided in the manuscript.

Field-specific reporting

Please select the one below that is the best fit for your research. If you are not sure, read the appropriate sections before making your selection.

☒ Life sciences ☐ Behavioural & social sciences ☐ Ecological, evolutionary & environmental sciences

For a reference copy of the document with all sections, see nature.com/documents/nr-reporting-summary-flat.pdf

Life sciences study design

All studies must disclose on these points even when the disclosure is negative.

Sample size	The sample sizes in this study are either number of bacterial strains tested (with replicates, see below), or # experimental or control cohort

Sample size	individuals taken from a publicly available dataset (for which sample size calculations were already performed). The specific # of bacterial strains used in this study (19) were chosen to allow for inclusion of major bacterial phyla within an individual donor microbiome, with replicates included to allow for statistical significance calculations. All sample sizes are listed in figure legends and methods sections where applicable.
Data exclusions	Data exclusion was based on sequencing coverage or genome quality to remove technical artifacts as described in the Methods section.
Replication	All in vitro assays on bacterial strains were performed with multiple (2-4) technical replicates, as noted in the methods section and figure legends where applicable, in order to confirm replicability and enable statistical signficance calculations.
Randomization	For all isolates generated in this study, individual of origins for isolated gut strains were assigned based on the defined identity of original feces (Table S2), for which covariate analysis is not applicable. For clinical datasets analyzed, cohort assignment for individuals was taken from the metadata of the original study.
Blinding	Blinding was not possible during experiments as we were comparing transcriptional responses of different bacterial isolates to different drug conditions. Transcriptomic and growth processing within species was blinded as different drug conditions were processed together using pooled methods. All analyses of associated data were performed with the same parameters and criteria described in Methods section.

Reporting for specific materials, systems and methods

We require information from authors about some types of materials, experimental systems and methods used in many studies. Here, indicate whether each material, system or method listed is relevant to your study. If you are not sure if a list item applies to your research, read the appropriate section before selecting a response.

Materials & experimental systems

n/a	Involved in the study
☒	☐ Antibodies
☒	☐ Eukaryotic cell lines
☒	☐ Palaeontology and archaeology
☒	☐ Animals and other organisms
☒	☐ Clinical data
☒	☐ Dual use research of concern

Methods

n/a	Involved in the study
☒	☐ ChIP-seq
☒	☐ Flow cytometry
☒	☐ MRI-based neuroimaging